Aalto University
School of Science and Technology
Faculty of Electronics, Communications and Automation
Department of Radio Science and Engineering

MARTTA-KAISA OLKKONEN

NON-DESTRUCTIVE RF MOISTURE MEASUREMENT OF BIO MATERIAL WEB

Thesis submitted in partial fulfillment of the requirements for the degree of Master of Science in Technology in Espoo _____._____._____

Supervisor	Professor Pertti Vainikainen
Instructor	Professor (Pro tem) Tommi Laitinen

Abstract

AALTO UNIVERSITY Abstract of the Master's Thesis

Author:	Martta-Kaisa Olkkonen
Name of the Thesis:	Non-destructive RF moisture measurement of bio material web
Date:	June 14, 2010 Number of pages: 72
Faculty:	Faculty of Electronics, Communications and Automation
Department:	Department of Radio Science and Engineering
Supervisor:	Professor Pertti Vainikainen
Instructor:	Professor (Pro tem) Tommi Laitinen

In this Master's thesis, it is studied, whether the moisture content of a bio material web can be measured non-destructively with a sensor by means of RF waves. The material under test is sludge from the process of a paper factory. The sludge is dewatered in a belt filter press because it will be burnt. The moisture content of the bio material web is of interest because the aim is to optimize energy consumption in the whole process.

A prototype sensor is built to perform test measurement both in laboratory conditions in Aalto University and finally in the factory in on-line conditions. The chosen resonator sensor is a strip-line cavity resonator. The frequency range over which the resonator functions is first tested with a reference material that is moistened with tap water. The operation of the resonator is tested also with two bio material samples in the laboratory. The operation of this resonator sensor is based on perturbation theory.

It can be estimated that the frequency shift caused by the material that is inserted in the resonator, is linear as a function of the water that the material contains. This applies to a situation where the imaginary part of the relative permittivity is much smaller than the real part.

In the factory measurements, 65 reference samples were collected and the corresponding resonant frequency shifts were measured. The analysis is based on the calculated equivalent thickness of the water layer. The relative shifts of the resonant frequency as a function of the equivalent water layer of each sample are fitted to a line. The result indicates that the standard deviation of the relative resonant frequency shift is 1.3%.

Keywords: resonator, moisture measurement, non-destructive testing, belt filter press

Tiivistelmä

AALTO-YLIOPISTO Diplomityön tiivistelmä

Tekijä:	Martta-Kaisa Olkkonen
Diplomityön nimi:	Biomateriaalirainan radiotaajuinen kosteudenmittaus ainetta rikkomatta
Päivämäärä:	14.6.2010 Sivumäärä: 72
Tiedekunta:	Elektroniikan, tietoliikenteen ja automaation tiedekunta
Laitos:	Radiotieteen ja –tekniikan laitos
Supervisor:	Professori Pertti Vainikainen
Instructor:	(m.a.) professori Tommi Laitinen

Tässä diplomityössä tutkitaan, onko ainetta rikkomaton, radiotaajuinen kosteudenmittaus mahdollista toteuttaa biomateriaalille, jolle menetelmää ei ole ennen käytetty. Tutkittava materiaali on lietettä paperiprosessista. Liete kuivatetaan suotonauhapuristimessa, koska aine menee poltettavaksi. Kosteudenmäärityksen avulla on tarkoitus optimoida koko prosessin energiankulutusta.

Sekä Aalto-yliopiston laboratorio-olosuhteissa että lopulta tehtaalla suoritettavia testimittauksia varten rakennettiin prototyyppianturi. Anturi on rakenteeltaan liuskajohdollinen onteloresonaattori. Anturin taajuusaluetta testattiin vertailunäytteellä, joka oli kasteltu hanavedellä. Myös biomateriaalinäytteitä testattiin laboratoriossa. Anturin toiminta perustuu perturbaatioteoriaan.

Voidaan tehdä oletus, että resonaattoriin asetetun materiaalin aiheuttama taajuusmuutos on suoraan verrannollinen aineen sisältämään kosteusmäärään. Oletus pätee silloin, kun suhteellisen permittiivisyyden imaginääriosa on huomattavasti pienempi kuin reaaliosa.

Tehdasmittausten aikana otettiin 65 näytettä ja vastaavat resonanssitaajuudet mitattiin anturilla. Tulosten jatkokäsittely perustuu laskettuun ekvivalentin vesikerroksen paksuuteen. Kunkin näytteen suhteellinen taajuuden muutos ekvivalentin vesikerroksen paksuuden funktiona sovitetaan suoralle. Päätellään, että suhteellisen taajuuden muutoksen standardideviaatio on 1.3%.

Avainsanat: resonaattori, kosteudenmittaus, ainetta rikkomaton testaus, suotonauhapuristin

PREFACE

I would like to thank professor Pertti Vainikainen for offering me this great, interesting subject for my Master's Thesis. The comments on how to proceed with the work were invaluable. Also the hints on how to improve the thesis itself were worth gold.

I would like to give my gratitude to my instructor Tommi Laitinen for guidance and for weekly and at times, daily, discussions on the project and my Master's Thesis.

Matti Saren from Metso Automation has coordinated the project ever since the beginning. Kimmo Kemppainen has been a contact person and a project leader from the side of UPM. Paavo Kumpula from UPM has been our host on the visits to the paper factory. I would like to thank Metso and UPM for the cooperation of the past seven months.

Eino Kahra had a huge rule in the design of the resonator sensor. Together with Pekka Rummukainen he made an assembly plan for the resonator. Pekka Rummukainen paid a visit to the factory to assemble the resonator to the belt filter press. Thank you, both, for helping me in anything concerning the mechanics of the measurement setup.

I would also like to thank Jan Järveläinen for his contribution to the project.

Finally, thanks to all in my family for encouraging me during my studies!

Martta-Kaisa Olkkonen

CONTENTS

LIST OF SYMBOLS

B_{3dB}	3 dB (half-power) bandwidth
$\bar{B}$	magnetic flux density vector
$\bar{D}$	electric flux density vector
$\bar{E}$	electric field strength vector
f_r	resonant frequency
f_{r0}	resonant frequency of an empty resonator
Δf_r	the change in the resonant frequency
$\bar{H}$	magnetic field strength vector
$\bar{J}$	electric current density vector
k	wave number
P	power
$\bar{P}$	dipole moment
Q	quality factor, electric charge
Q_d	dielectric loss factor
Q_l	loaded quality factor
Q_r	quality factor of an empty resonator
Q_u	unloaded quality factor

W	energy
α	the attenuation constant
β	the phase constant
$\tan \delta$	the loss tangent
ε	permittivity
ε_0	permittivity in vacuum
ε_r	relative permittivity
ε_r'	real part of complex relative permittivity
ε_r''	imaginary part of complex relative permittivity
λ	wavelength
μ	permeability
μ_0	permeability in vacuum
μ_r	relative permeability
ω	angular frequency
ρ	electric charge density
σ	conductivity or standard deviation

ABBREVIATIONS

EHF	extremely high frequencies
EM	electromagnetic
HF	high frequencies
LF	low frequencies
MF	medium frequencies
MUT	material under test
RF	radio frequency
SHF	super high frequencies
TE	transverse electric field
TM	transverse magnetic field
UHF	ultra high frequencies
VHF	very high frequencies
VLF	very low frequencies
VNA	vector network analyzer

CHAPTER 1

INTRODUCTION

There is a need for fast and accurate moisture measurement in different fields of industry. The measured object may be paper on a paper machine or for example plywood in its production line. Some of the traditional moisture definition methods, such as the oven-drying method, have the disadvantage of being time-consuming and sometimes inaccurate. Some other methods, on the other hand, may disadvantageously require touching the material during the measurement. In this work, moisture measurement based on the use of radio-frequency (RF) waves, is considered. One of the major advantages of using RF waves for moisture measurement is that it becomes possible to perform the measurement non-destructively, without touching the measured object. In other words, the material under test (MUT) is by no means affected by the measurement. This is very important, when the properties of fragile or thin sheets of, for example, paper are being measured.

This work deals with moisture measurement of a bio material web non-destructively using RF waves. In more detail, the term 'bio material' means here the material from a biological waste management system in a paper or pulp factory. The material is sludge from the process of the paper or pulp factory and it is then dewatered in a belt filter press, so that it becomes a solid bio material web. Such bio material can potentially be or is burnt and used for energy. Therefore it becomes of natural interest to consider how the material should or could be pre-processed to optimize the benefits from its burning, and in this context (controlling of) the moisture content of the material is in a central role. Hence, it becomes useful to monitor the moisture content of the bio material by measurement and in this way enable the controlling of the process.

The purpose of this work is to examine whether or not the on-line RF moisture measurement is successful for the bio material in question. A well-known stripline cavity resonator structure is used [13]. A specific goal is to study, whether the properties of the bio material allow the RF moisture measurement reliably. The planned frequency of operation of the sensor is approximately 400 MHz.

Ch. 2 introduces the background electromagnetic theory and the material parameters of which the relative permittivity is of interest in this thesis. In Ch. 3 the most common sensor types are presented, but the focus is on resonator sensors. The perturbation theory for the strip-line resonator is presented. In Ch. 4 the factory measurements are

described; the measurement setup and the main results after the analysis. The samples that were taken in the factory and the corresponding resonance measurement results are processed; the frequency shift due to the material as a function of the water content of the samples is presented in a figure. Based on the perturbation theory of strip-line resonators, the results are fitted to a line. The conclusions are summed up in Ch. 5.

CHAPTER 2

BACKGROUND ELECTROMAGNETIC THEORY

In this chapter the background electromagnetic theory and equations related to them are discussed in Sec. 2.1. The theory of this chapter is based on Refs. [1] – [5]. The notation that is used is the same as in these references. In Sec. 2.2 the equations for the complex permittivity of water are presented and plotted as a function of frequency.

2.1 Electromagnetic waves

Microwave frequency region covers the frequencies from 300 MHz to 300 GHz. This band further consists of UHF, SHF and EHF regions as indicated in Table 2.1.

Table 2.1. Frequency regions of radio waves [1].

VLF	Very Low Frequencies	3-30kHz
LF	Low Frequencies	30-300kHz
MF	Medium Frequencies	300-3000kHz
HF	High Frequencies	3-30MHz
VHF	Very High Frequencies	30-300MHz
UHF	Ultra High Frequencies	300-3000MHz
SHF	Super High Frequencies	3-30GHz
EHF	Extremely High Frequencies	30-300GHz
Sub millimeter waves		300-3000 GHz

The wavelength is calculated from (2.1) [2]

$$\lambda = \frac{c}{f} \tag{2.1}$$

where c is the speed of light and f is the frequency. In vacuum the speed of light is approximately $c_0 = 3 \cdot 10^8 \frac{m}{s}$. In the microwave region the wavelength is thus between 1 mm and 1 m.

In the microwave region the frequency is relatively high and the wavelength rather short. Microwave components are often distributed elements. This means that the dimensions of the device under test are on the order of the microwave wavelength. Therefore lumped element approximations are not valid at microwave frequencies. In this case standard circuit theory cannot be used to solve microwave problems [2].

Electric and magnetic phenomena at a macroscopic level are described by Maxwell's equations (2.2) – (2.5) [3] that were published in 1873.

$$\nabla \cdot \bar{D} = \rho \tag{2.2}$$

$$\nabla \cdot \bar{B} = 0, \tag{2.3}$$

$$\nabla \times \bar{E} = \frac{-\partial \bar{B}}{\partial t} \tag{2.4}$$

$$\nabla \times \bar{H} = \frac{-\partial \bar{D}}{\partial t} + \bar{J} \tag{2.5}$$

where $\bar{E}$ is the electric field density [V/m], $\bar{H}$ is the magnetic field density [A/m], $\bar{D}$ is the electric flux density [C/m^2], $\bar{B}$ is the magnetic flux density [Wb/m^2], $\bar{J}$ is the electric current density [A/m^2], ρ is the electric charge density [C/m^3]

In the above equations the sources of the electromagnetic fields are current density $\bar{J}$ and the electric charge ρ [1].

In order to solve electromagnetic problems it is necessary to know the following relations that hold information about the medium in which the electromagnetic (EM) wave propagates. The relations between electric and magnetic field densities (2.6) [1] and flux densities (2.7) [1] are

$$\bar{B} = \mu_0 \mu_r \bar{H}, \tag{2.6}$$

$$\bar{D} = \varepsilon_0 \varepsilon_r \bar{E}, \tag{2.7}$$

where μ_r is the relative permeability, $\mu_0 = 4\pi \cdot 10^{-7} \frac{H}{m}$ is the permeability of free-space, ε_r is the relative permittivity and $\varepsilon_0 = 8.854 \cdot 10^{-12} \frac{F}{m}$ is the free-space permittivity [1].

2.1.1 Time-harmonic fields

The Maxwell's equations are also presented for time-harmonic fields which means that the waves are sinusoidally time-varying. The Euler's formula is defined as $e^{j\omega t} = \cos \omega t + j \sin \omega t$ [4], where $\omega = 2\pi f$ is the angular frequency in radians and $j = \sqrt{-1}$ is the imaginary unit. Taking into account the Euler's formula, time-harmonic fields can be presented as (2.8) [4]

$$\bar{A}(x, y, z, t) = Re[\bar{A}(x, y, z)e^{j\omega t}] \tag{2.8}$$

Since the time derivatives are always directed to the term $e^{j\omega t}$, they can be replaced in a following way for the first order (2.9) [4] and second order (2.10) [4] derivatives.

$$\frac{\partial}{\partial t} \rightarrow j\omega \tag{2.9}$$

$$\frac{\partial^2}{\partial t^2} \rightarrow (j\omega)^2 = -\omega^2 \tag{2.10}$$

and so on for higher order derivatives.

By using the dependencies (2.6) and (2.7) and replacing the time derivatives according to (2.9) the time-harmonic Maxwell's equations are (2.11) – (2.14) [3].

$$\nabla \cdot \bar{D} = \rho \tag{2.11}$$

$$\nabla \cdot \bar{B} = 0, \tag{2.12}$$

$$\nabla \times \bar{E} = -j\omega\bar{B} = -j\omega\mu\bar{H} \tag{2.13}$$

$$\nabla \times \bar{H} = j\omega\bar{D} + \bar{J} = (\sigma + j\omega\varepsilon)\bar{E} \tag{2.14}$$

In Eq. (2.14) has been taken into account that Ohm's law from an electromagnetic field's point of view can be written (2.15) [3]

$$\bar{J} = \sigma\bar{E}, \tag{2.15}$$

where σ is the conductivity [$\frac{S}{m} = \frac{A}{Vm}$] of the medium.

It can be noticed that there is no time dependency in Eqs. (2.11) – (2.14) because $e^{j\omega t}$ has been removed from the equations.

The complex propagation constant of a plane wave is (2.16) [3]

$$\gamma = \alpha + j\beta = j\omega\sqrt{\mu\varepsilon}\sqrt{1 - j\frac{\sigma}{\omega\varepsilon}}, \tag{2.16}$$

where α is the attenuation constant, β is the phase constant and σ is the conductivity.

2.1.2 Fields in media, losses

In the preceding equations it was assumed that no material bodies were present. Fields that propagate in media can be analyzed in the following way.

If a piece of material is placed in an electrical field $\bar{E}$, the material will become polarized; the positively and negatively charged particles will move to opposite directions.

In the case of a plate capacitor, charges $+Q$ and $-Q$ create an electric flux density $\bar{D}$ between the plates. The relation between $\bar{E}$ and $\bar{D}$ in vacuum is, Eq. (2.17) [5]

$$\bar{E} = \frac{1}{\varepsilon_0}\bar{D} \tag{2.17}$$

When a piece of material is inserted between the capacitor plates, the charged particles will move in the direction of the plates. This displacement of charges is described by the dipole moment $\bar{P}$. The electric dipole moment is a vector pointing in the opposite direction than the electric flux density, and thus partly counteracts it. Therefore the mean electric field $\bar{E}_i$ inside the dielectric is lower (2.18) [5]

$$\bar{E}_i = \frac{1}{\varepsilon_0}(\bar{D} + \bar{P}) \tag{2.18}$$

The effect of polarization is usually written as the change of the permittivity (2.19)

$$\bar{E}_i = \frac{1}{\varepsilon_0}(\bar{D} + \bar{P}) = \frac{1}{\varepsilon}\bar{D} = \frac{1}{\varepsilon_r\varepsilon_0}\bar{D} \tag{2.19}$$

$\varepsilon_r = \frac{\varepsilon}{\varepsilon_0}$ is the relative permittivity which describes how easily the medium is polarized.

The complex permittivity is (2.20) [3]

$$\varepsilon = \varepsilon_0\varepsilon_r = \varepsilon' - j\varepsilon'' = \varepsilon_0(\varepsilon_r' - j\varepsilon_r''), \tag{2.20}$$

where ε' is the real part and ε'' the imaginary part of the dielectric constant. The imaginary part of the dielectric constant ε'' is a measure of how dissipative a medium is. It gives the rate of attenuation to a propagating wave. If $\varepsilon'' = 0$, the medium is lossless. The real part ε' affects the electric field of a propagating wave and changes the ratio between the electric and magnetic field strengths. The ε' also decreases the speed of propagation which can be seen from Eq. (2.21) [5].

$$c = \frac{c_0}{\sqrt{\varepsilon_r'}} \tag{2.21}$$

Equation (2.21) describes the speed of propagation in a nonmagnetic, lossless medium.

In addition to dielectric damping, the losses in media can also be caused by the conductivity σ of the material. In this case there are free charges in the material that are moved by the electric field.

When $\bar{J} = \sigma\bar{E}$ and Eq. (2.7) are inserted to Maxwell's curl equation (2.14), it becomes to the following form (2.22) [1]

$$\nabla \times \bar{H} = j\omega\bar{D} + \bar{J} = j\omega(\varepsilon' - j\varepsilon'' - j\frac{\sigma}{\omega})\bar{E} \tag{2.22}$$

In Eq. (2.22) it can be noticed that the loss due to dielectric damping ($\omega\varepsilon''$) is distinguishable from conductivity loss (σ).

For microwave materials a quantity of interest is the loss tangent. The loss tangent (2.23) [1] can be defined based on (2.22)

$$\tan\delta = \frac{\omega\varepsilon'' + \sigma}{\omega\varepsilon'} \tag{2.23}$$

Also, using (2.23), $\tan\delta$ can be used to define complex permittivity (2.24) [1]

$$\varepsilon = \varepsilon' - j\varepsilon'' = \varepsilon'(1 - j\tan\delta) \tag{2.24}$$

Hence, microwave materials can be characterized by specifying the real permittivity, $\varepsilon' = \varepsilon_r'\varepsilon_0$, and the loss tangent at a certain frequency.

2.2 The permittivity of water

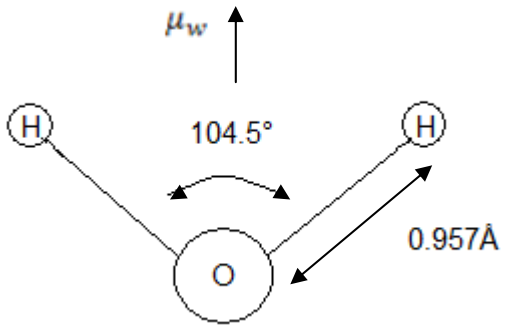

Figure 2.1. The water molecule.

Liquid water is a polar substance. The water molecule, which is illustrated in Fig. 2.1, has a permanent dipole moment $\mu_w = 6.14 \cdot 10^{-30}$ Asm [5].

The frequency dependence of the permittivity of a polar material is given by the Debye relation (2.25) [5]

$$\varepsilon_r = \varepsilon_\infty + \frac{\varepsilon_s - \varepsilon_\infty}{1 + j\omega\tau} \tag{2.25}$$

where ε_s is the static permittivity (i.e. the value at zero frequency), ε_∞ is the permittivity at such high frequencies that orientation polarization does not have time to develop and τ is the time constant (i.e. the time that it takes for dipoles to revert to random orientation, when the electric field is removed).

If the liquid contains also ions for example in electrolytic solution, the conductivity term must be added to the Debye relation, Eq. (2.26) [5]

$$\varepsilon_r = \varepsilon_\infty + \frac{\varepsilon_s - \varepsilon_\infty}{1 + j\omega\tau} - j\frac{\sigma}{\omega\varepsilon_0} \tag{2.26}$$

In Fig. 2.2 the real and negative imaginary part of the complex permittivity of water are represented as a function of frequency. Equation (2.25) is plotted over a wide band from 100 MHz to 1000 GHz with values $\varepsilon_\infty = 4.9$, the salinity 0 % and the temperature 20 °C. The values for ε_s, τ and σ are calculated from equations that are taken from [5].

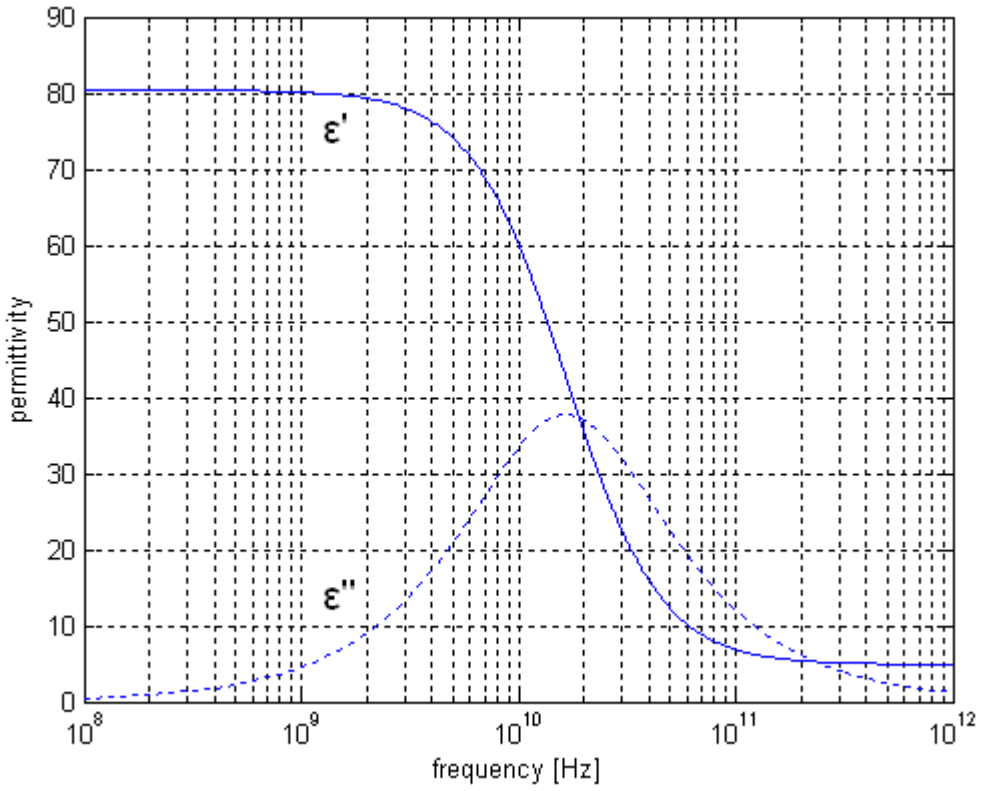

Figure 2.2. The complex permittivity of water. The solid line represents the real part (ε') and the dashed line represents the negative imaginary part (ε'').

In Fig. 2.2 it is seen that the permittivity undergoes dispersion and dielectric losses occur at the relaxation frequency $\omega = 1/\tau$ (approximately 20 GHz).

The salinity of ocean water is approximately 3.5%. To represent the complex dielectric spectrum of salt water in Fig. 2.3, the ion conductivity has to be taken into account, as in Eq. (2.26). The same equations for ε_s, τ and σ are used for salt water, but now the salinity S is 3.5%.

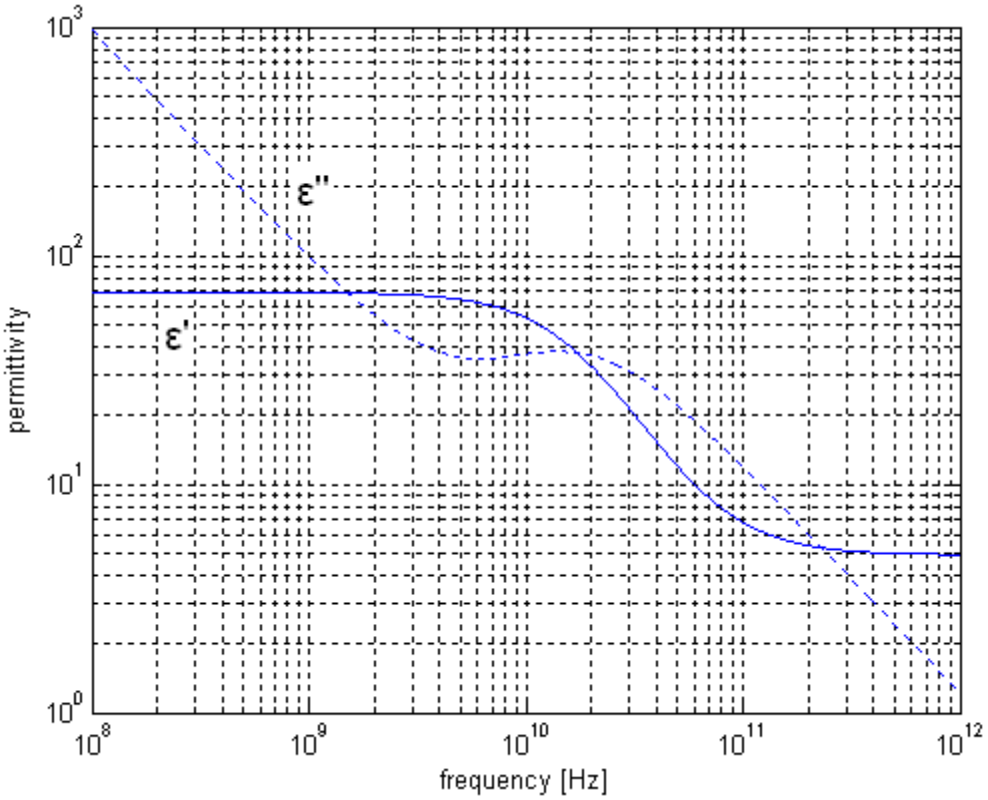

Figure 2.3. The complex permittivity of salt water with salinity of 3.5%.

CHAPTER 3

THEORY OF MOISTURE MEASUREMENT, SENSOR TYPES AND CHOOSING THE SENSOR

In this chapter the theory of moisture measurement and the possible moisture sensors is discussed, based on Refs. [2] - [9]. In Sec. 3.1 some of the most important microwave sensors are presented. In Sec. 3.2 the resonator as a sensor is introduced and the resonance phenomenon is presented. The chosen sensor type for the moisture measurement of this thesis is a resonator sensor, and in detail, a strip-line resonator sensor. The perturbation theory of strip-line resonators is in Sec. 3.3. The theory of moisture measurement is presented in Sec. 3.4.

3.1 Sensors

This section is organized as follows. Subsection 3.1.1 discusses the transmission sensors, Subsection 3.1.2 presents the reflection sensors and 3.1.3 the concept of sensor arrays.

3.1.1 Transmission sensors

Transmission sensors consist of a radio transmitter and a receiver. If a piece of dielectric material is placed between the transmitting and receiving antennas, the amplitude of the signal is decreased and the phase is changed.

Fig. 3.1 (a) [6] presents a free space transmission sensor. They are simple; they consist only of a pair of horn antennas, a microwave source and a detector. In an on-line measurement the MUT can be measured directly from a conveyor belt.

Fig. 3.1 (b) [6] shows a method based on transmission lines; the MUT is placed near a transmission line, in this case a microstrip line, and the wave propagating through the line is affected by the MUT. The amplitude of the wave is attenuated and the phase is delayed by the moisture contained in the material.

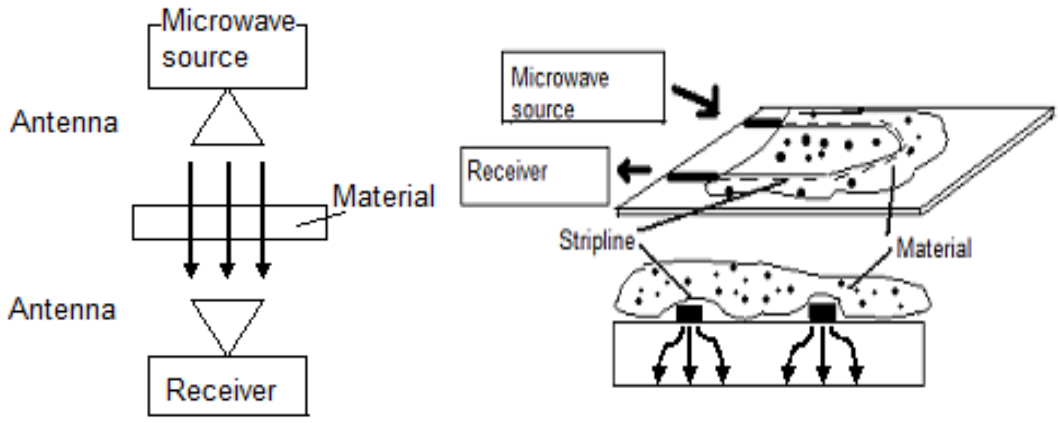

(a) (b)

Figure 3.1. (a) Free space method **(b)** Transmission method.

Transmission sensors are best suited for measuring high loss materials [5].

3.1.2 Reflection sensors

A simple reflection sensor is an open end of a transmission line, for example a coaxial cable or a waveguide. Reflection sensors allow one-sided sensing. The open end of the transmission line is pressed against or brought in the vicinity of the MUT to measure the reflection coefficient, which depends on the end capacitance and conductance. The capacitance and conductance are functions of the relative permittivity ε_r. One application for reflection sensors is measurement of ground moisture [3]. Figure 3.2 shows three different open-ended transmission line structures used as sensors: a microstrip line, a coaxial line and a cylindrical waveguide.

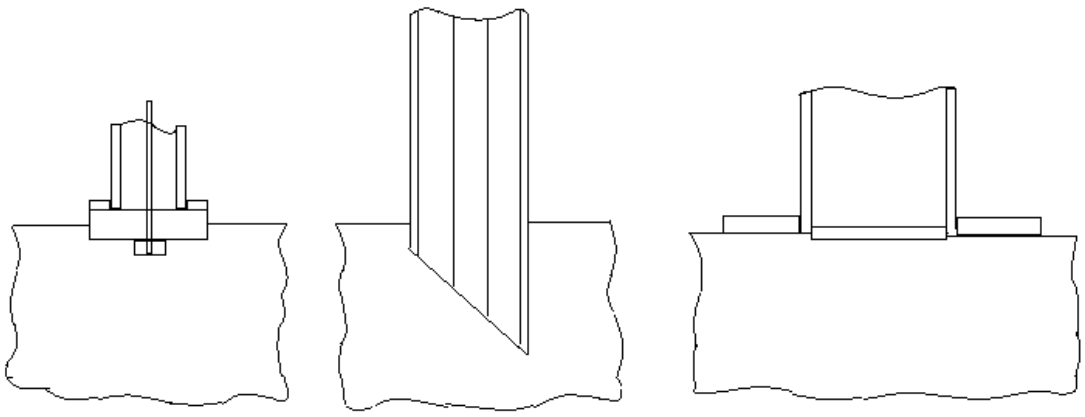

Figure 3.2. From left to right: a microstrip line, a coaxial line and a cylindrical waveguide.

3.1.3. Sensor arrays

Sensor arrays are needed, when the properties of wide and rapidly moving objects are measured. They can be for example sheets of paper or veneer on a conveyor belt. Arrays of sensors are constructed of, for example, multiple similar resonator sensors, which have the same resonant frequency. The measurement speed reduces, if the resonant frequencies deviate from each other. The coupling between adjacent sensors can be avoided by using switches that allow only one sensor to resonate at a time [8].

Resonator sensors are discussed in detail in Sec. 3.2.

3.2 Resonator sensors

3.2.1 Resonance phenomenon

In circuit theory a resonator is formed of lumped elements: coils, capacitors and resistors. Only the values of the elements affect the frequency response of the resonator. For more complex (e.g. three dimensional) structures a basic circuit model may, however, become too simplified [4].

A resonator is a structure that has a natural frequency of oscillation, a resonant frequency (3.1) [3].

$$f_r = \frac{1}{2\pi\sqrt{LC}} \tag{3.1}$$

A simple resonator can be formed only of one capacitor, C, and inductor, L (Fig. 3.3) [3].

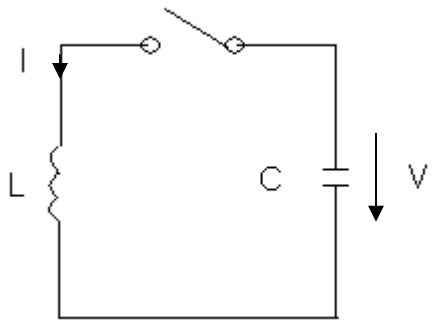

Figure 3.3. A simple resonator composed of inductor L and capacitor C.

At first, the switch is open and the capacitor is charged (Fig. 3.3) [3]. The electric field of the capacitor contains an energy $W_e = \frac{CV^2}{2}$. The current I starts flowing through the coil, when the switch is closed. When the energy has moved entirely to the coil, its energy is $W_m = \frac{LI^2}{2}$.

A resonance occurs when the average energy in the electric field is equal to the average energy in the magnetic field, $W_e = W_m$.

3.2.2 Losses in resonators, quality factor

The resonator is never ideal and lossless as in Fig. 3.3. The losses of a resonator are modeled with a parallel conductance G in a parallel resonant circuit and with resistance R in a series resonant circuit, Fig. 3.4 [3].

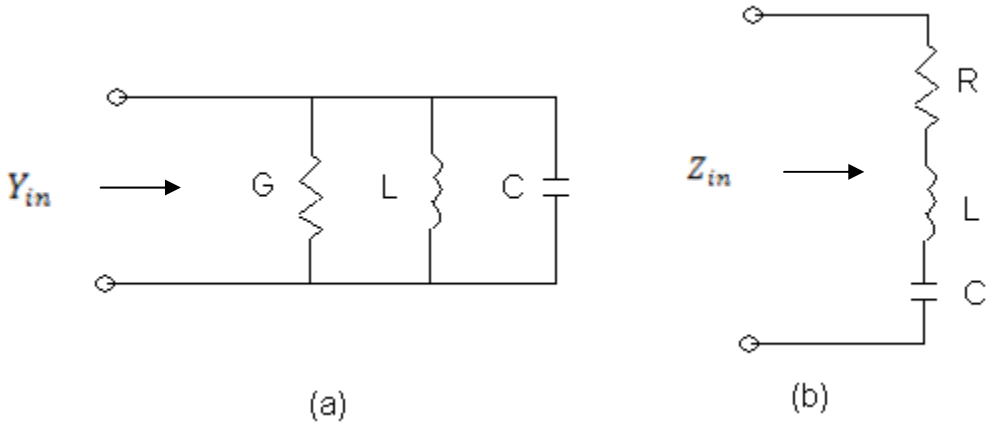

Figure 3.4. (a) A parallel and **(b)** a series resonant circuit.

The quality factor Q is a measure of loss for resonators. The higher is the Q, the lower the loss. Also, the Q is a figure of merit of how selective the resonator is.

The definition of the quality factor is (3.2) [3]

$$Q = \frac{\omega_r W}{P_l}, \tag{3.2}$$

where ω_r is the angular resonant frequency, W is the energy stored in the resonator and P_l is the power loss in the resonator.

The Q can also be defined by using half-power frequencies (3.3) illustrated in Fig. 3.5 [3].

$$Q = \frac{\omega_r}{2\Delta\omega_{3dB}} = \frac{f_r}{2\Delta f_{3dB}} \tag{3.3}$$

In Fig. 3.5 $P_{l,max}$ is P_l at the resonant frequency.

It can be seen from Eq. (3.3) that Q is inversely proportional to the bandwidth of the resonance plot.

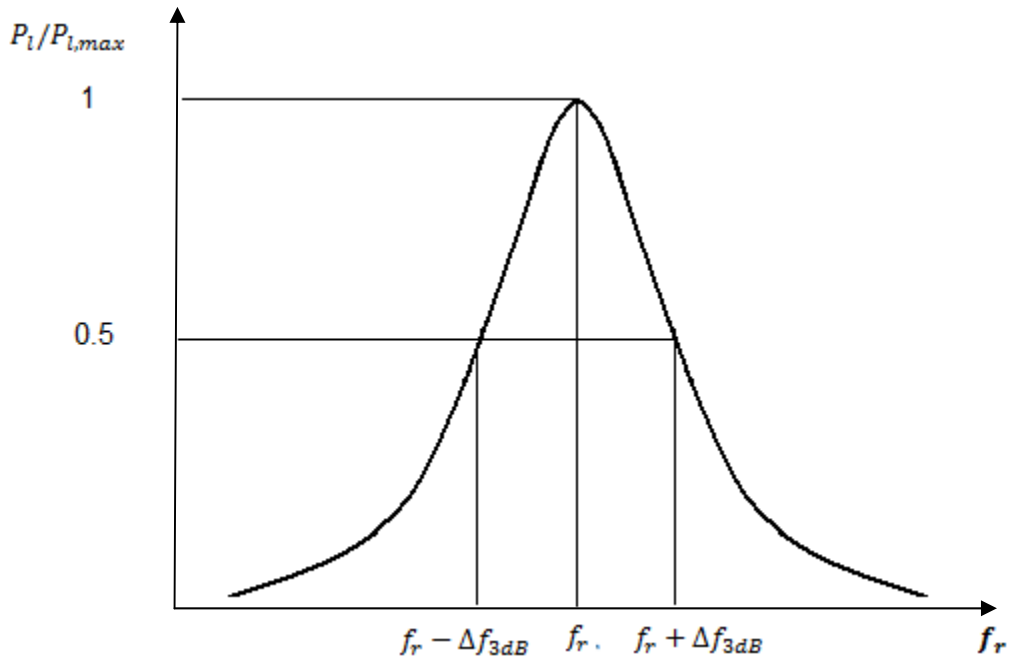

Figure 3.5. Power absorbed in a resonator.

The Q defined in (3.2.) and (3.3) was a characteristic of the resonant circuitry itself without any external loading effects. If the resonant circuitry is coupled to an external load, the overall Q will be lowered. The loaded Q, Q_L, can be solved from (3.4) [2]

$$\frac{1}{Q_L} = \frac{1}{Q_u} + \frac{1}{Q_e}, \tag{3.4}$$

where Q_u is the unloaded Q related to the loss in the resonator. Q_e is the external Q, when the resonator is coupled to an external load.

3.3 The permittivity of a material as a function of the resonant frequency and the quality factor

The resonant frequency and the quality factor of a resonator change, when dielectric material is inserted into the resonator. The change is proportional to the square of the electric field strength at the location of the object. The electric field pattern is determined by the structure of the resonator. In the following section, the field patterns are presented for a stripline resonator. For example, a stripline resonator with one center conductor supports one first order resonant mode. A resonator with two center conductors has either one or two first order resonant modes.

3.3.1 Perturbation theory

In this subsection the perturbation theory is presented. The equations for calculating the complex permittivity from the resonant frequency and the quality factor are introduced.

The perturbation theory provides equations for calculating the resonant frequency shift, when the material sample to be measured fills only a small portion of the resonator. The perturbation theory applies also to larger samples if the permittivity is low. The general, exact perturbation formula is (3.5) [5]

$$\frac{\omega_{r2}-\omega_{r1}}{\omega_{r2}} = -\frac{\int_v [(\varepsilon_{r2}-\varepsilon_{r1})\varepsilon_0\bar{E}_2\cdot\bar{E}_1^*+(\mu_{r2}-\mu_{r1})\mu_0\bar{H}_2\cdot\bar{H}_1^*]dV}{\int_v [\varepsilon_{r1}\varepsilon_0\bar{E}_2\cdot\bar{E}_1^*+\mu_{r1}\mu_0\bar{H}_2\cdot\bar{H}_1^*]dV}. \tag{3.5}$$

Equation (3.5) applies to a situation where the permeability (μ) as well as the permittivity (ε) changes. Subscript 1 refers to the situation before and subscript 2 after inserting the sample to be tested.

A few approximations can be made in order to derive the formulas for some practical situations. The μ is assumed to be constant. It can be noticed that in (3.5) the denominator is the total energy in the resonator. The denominator can be substituted by twice the value of the first term in it. Equation (3.5) can be simplified [5]

$$\frac{\Delta\omega_r}{\omega_r} \approx -\frac{\int_v (\varepsilon_{r2}-\varepsilon_{r1})|E|^2dV}{2\int_v \varepsilon_{r1}|E|^2dV}. \tag{3.6}$$

Equation (3.6) comes to the following form (3.7), when it is assumed that $\varepsilon_{r1} = 1$ and ε_{r2} is constant in the sample

$$\frac{\Delta\omega_r}{\omega_r} \approx -\frac{(\varepsilon_r-1)\int_{vs}|E|^2dV}{2\int_v |E|^2dV} = -\frac{(\varepsilon_r-1)}{2}S, \tag{3.7}$$

where the ratio of the integrals, S, is the filling factor. The subscript vs refers to the volume of the sample and v to the whole resonator.

In the following cases, the sample is lossy and the change in the angular frequency becomes complex. When the electric field is tangential to the sample, (3.7) comes to the following form

$$\frac{\Delta\omega_r}{\omega_r} \approx -\frac{(\varepsilon_r'-1-j\varepsilon_r'')}{2}\cdot\frac{\int_{vs}|E|^2dV}{\int_v |E|^2dV} = -\frac{(\varepsilon_r'-1)}{2}S + j\frac{\varepsilon_r''}{2}S. \tag{3.8}$$

The following approximations for the relative change of frequency (3.9) and the change of $1/Q_l$ (3.10) [5] are achieved for the tangential electric field, which is also called the even wave mode.

$$\frac{\Delta f_r}{f_r} \approx -\frac{\varepsilon_r'-1}{2} \cdot S \tag{3.9}$$

$$\Delta\left(\frac{1}{Q_l}\right) \approx \varepsilon_r'' \cdot S \tag{3.10}$$

In the case where the external electric field is perpendicular to the surface of the sample, the boundary condition is $E_i = E_e/\varepsilon_r$. This wave mode is called the odd mode. The subscript i refers to the internal and e to the external electric field.

From (3.7) and the boundary conditions Eq. (3.11) is deduced

$$\frac{\Delta\omega_r}{\omega_r} \approx -\frac{(\varepsilon_r-1)}{2\varepsilon_r} S \approx -\frac{(\varepsilon_r'-1)}{\varepsilon_r'} \cdot \frac{S}{2} + j\frac{\varepsilon_r''}{(\varepsilon_r')^2} \cdot \frac{S}{2} \tag{3.11}$$

For the odd mode, the change of frequency and $1/Q_l$ are the following (3.12) and (3.13) [5]

$$\frac{\Delta f_r}{f_r} \approx -\frac{\varepsilon_r'-1}{2\varepsilon_r'} \cdot S \tag{3.12}$$

$$\Delta\left(\frac{1}{Q_l}\right) \approx \frac{\varepsilon_r''}{(\varepsilon_r')^2} \cdot S \tag{3.13}$$

Equations (3.12) and (3.13) apply when $\varepsilon_r'' < 0.1\varepsilon_r'$.

3.3.2 Even and odd resonant modes

In [8] the resonance modes are presented for a stripline resonator. A $\lambda/2$ stripline resonator, i.e. a section of stripline with either open or short-circuited ends, supports both even and odd (quasi-TEM) resonance modes. A $\lambda/4$ stripline resonator has only the even resonant mode. For the $\lambda/4$ resonator the other end is open and the other short-circuited. The electric field distribution for a $\lambda/2$ two-conductor stripline resonator is presented in Fig. 3.6 [8]. The electric potentials of the center conductors are equal for the even mode but they have opposite signs for the odd mode. The electric field is perpendicular to the material layer for the odd mode and parallel to the material in the middle of the center conductors.

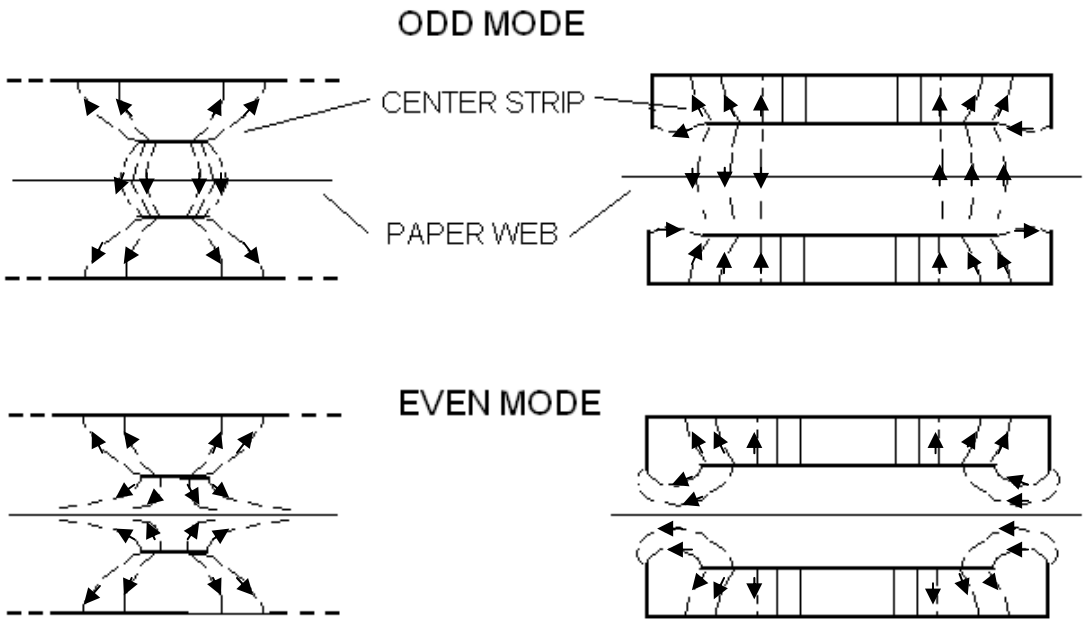

Figure 3.6. The electric field patterns for a $\lambda/2$ two-conductor stripline resonator, for odd and even modes.

For the even mode the change in f_{r0} (the resonant frequency of an empty resonator) depends linearly on the permittivity $(\varepsilon_r' - 1)$. For the odd mode the frequency shift is proportional to $((\varepsilon_r' - 1)/\ \varepsilon_r')$. When the permittivity is small, the frequency shifts are quite the same for both wave modes. When the permittivity becomes larger, the frequency change is quickly saturated for the odd mode [10]. Therefore, the odd mode is not suitable for measuring the properties of materials with high moisture [8].

The permittivity of the moist bio material under test is rather large. The resonator sensor which is designed in this thesis is planned to support the even mode and be linear as a function of $(\varepsilon_r' - 1)$.

3.4 Moisture measurement with a resonator sensor

In this section the theory of moisture measurement is presented. Very often, the moisture content of many kinds of materials is needed to know in different fields of industry. One of the major advantages of using microwaves for moisture measurement is that the method is non-destructive. This means, that the MUT is by no means affected by the measurement. This is very important, when the properties of very fragile and thin sheets of e.g. paper are measured.

To measure the moisture content of the bio material, a resonator sensor was chosen. The theory of the resonance phenomenon is in Sec. 3.2. The design process and final structure of the resonator are described in detail in Ch. 4.

In Sec. 3.4.2 the equations for calculating the resonant frequency and the quality factor of a resonator are given. The assumption is made for the bio material, the MUT in this thesis, that the real part of the complex relative permittivity is much larger than the imaginary part $\varepsilon_r' \gg \varepsilon_r''$. For nonmagnetic materials $\mu_r = 1$, which is assumed in the rest of this thesis.

3.4.1 Defining the moisture content

When using the wet basis, the term *moisture content* refers to the ratio of water to the total mass of wet material. The term *water content* is the amount of water in a certain amount of material [9]. The moisture content of a material can be defined by either wet basis (w.b) or dry basis (d.b.).

Equation (3.14) is the moisture content by wet basis ξ [9]

$$\xi = \frac{m_w}{m_m} = \frac{m_w}{m_w + m_d}, \tag{3.14}$$

where m_w is the mass of water, m_d is the mass of dry material and m_m is the total mass of the wet material.

The moisture content defined by dry basis (d.b), η, is obtained from (3.15) [9]

$$\eta = \frac{m_w}{m_d} = \frac{m_m - m_d}{m_d}. \tag{3.15}$$

3.4.2 The resonant frequency and the quality factor of a resonator sensor

The attenuation or phase shift caused by the water contained in materials is used to determine the moisture content. The electromagnetic wave is affected by the relative permittivity of the material which is related to the water content of the material.

The resonant frequency and quality factor can be measured either by the method of reflection coefficient or transmission coefficient. The former method requires only one coupling and the latter requires two couplings.

In the method of reflection loss a wave is transmitted along a cable toward the resonator. The reflected power is measured and the amplitude and the phase of the reflection coefficient can be calculated. The method of insertion loss means that the field in the resonator is excited through one coupling and measured through the other coupling. In Fig. 3.7 (b) a is the insertion loss which is the ratio of the received power and the incident power, $\frac{P_t}{P_i}$ [5].

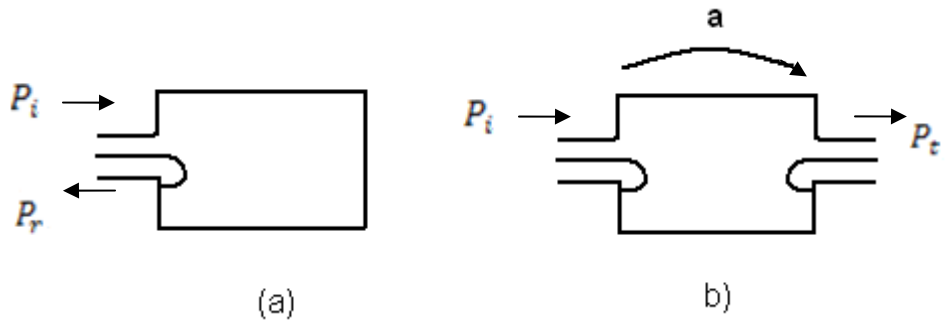

Figure 3.7. Coupling in the method of **(a)** reflection loss **(b)** insertion loss.

The method of insertion loss is used in this thesis.

If the couplings of Fig. 3.7 (b) are equal, the insertion loss a (3.16) and the phase shift (3.17) [5] can be calculated

$$a = \frac{\left(1-\frac{Q_l}{Q_u}\right)^2}{1+Q_l^2\left(\frac{f}{f_r}-\frac{f_r}{f}\right)^2} \tag{3.16}$$

$$\varphi = \varphi_0 - \arctan\left[Q_l\left(\frac{f_r}{f}-\frac{f}{f_r}\right)\right], \tag{3.17}$$

where the constant φ_0 is either 0° or 180° if only one type of coupling is used. From Eqs. (3.16) or (3.17) f_r and the quality factor Q_l can be solved.

The loaded quality factor can be calculated from the half-power frequencies, Eq. (3.3). If the couplings on both sides are equal, the unloaded quality factor can be calculated from (3.18) [5]

$$Q_u = \frac{Q_l}{1-\sqrt{a_r}}, \tag{3.18}$$

where a_r is the insertion loss at the resonant frequency.

To determine the permittivity as a function of f_r and Q, the following simple equations can be used.

$$\varepsilon_r' \approx \left(\frac{f_{r0}}{f_r}\right)^2 \tag{3.19}$$

$$\frac{1}{Q_d} = \tan\delta = \frac{\varepsilon_r''}{\varepsilon_r'}, \tag{3.20}$$

where f_{r0} is the resonant frequency of an empty resonator and f_r is that of a filled one. They apply to a situation where a resonator has an electric field volume that is completely filled with the material to be measured.

Equation (3.19) combines the real part of the relative permittivity to f_r and Eq. (3.20) the complex permittivity to the dielectric loss factor, Q_d. Q_d is related to the losses caused by inserting a piece of dielectric material into the resonator. Equation (3.19) is an approximation for the case when $\varepsilon_r' \gg \varepsilon_r''$ [5].

CHAPTER 4

EXPERIMENTS

This chapter discusses the experiments with the sensor prototype. In Sec. 4.1 the process of designing the sensor is described. A prototype resonator sensor is built and tested in the laboratory in Aalto University. The frequency range of operation of the resonator is defined with a reference material, which is described in Sec. 4.2. In Sec. 4.3 the bio material is tested as well. The results from the factory measurements are analyzed in Sec. 4.4.

4.1 The sensor structure

The design process of the sensor was started with a known resonator structure that is in commercial use in the VITKA sensor. The acronym comes from the Finnish words *viilun tiheys- ja kosteusanturi.* The structure of the resonator sensor has been simulated in the special assignment of Tony Niemi [13]. In this section, the important results are reported, that can be applied when the resonator sensor of this thesis is designed and built.

The material of the resonator cavity and the center conductor is aluminum and the dimensions of the resonator are presented in Figs. 4.1 and 4.2 [13].

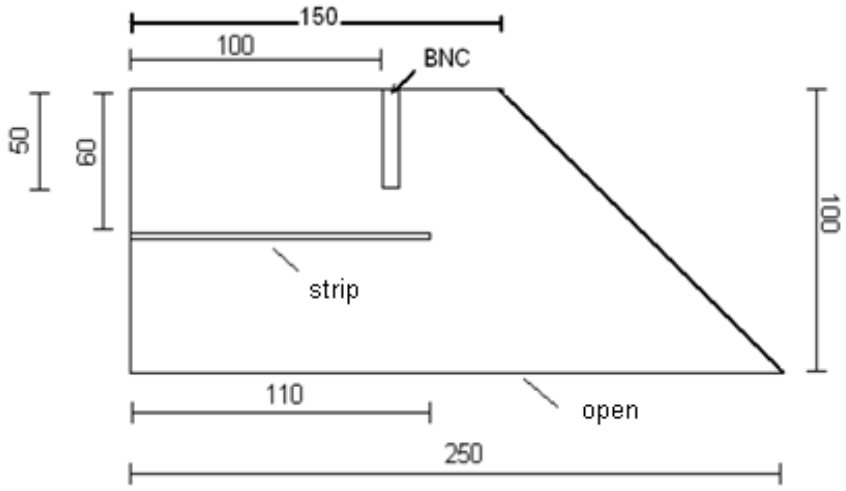

Fig 4.1. Side view of a resonator half. Measures are in millimeters [13].

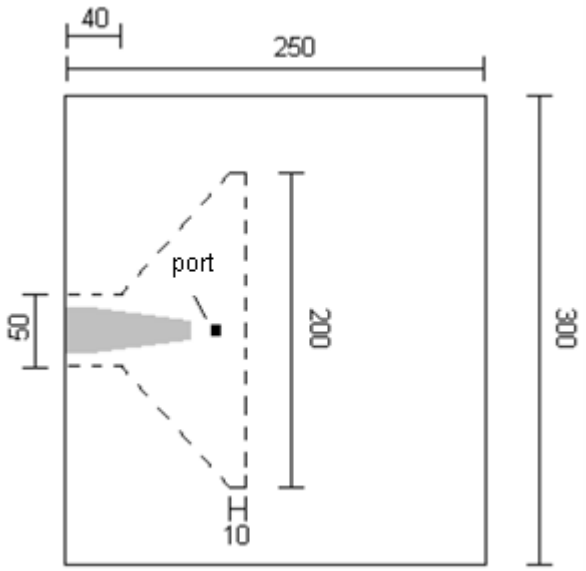

Fig 4.2. Top view of the resonator. Measures are in millimeters [13].

In Fig. 4.1 the side view of the resonator half is presented. Figure 4.2 shows the top view of the resonator. All the dimensions are in millimeters. Both resonator halves are identical. In the simulations, the MUT flows through the resonator, between the resonator halves. The signal is fed to the resonator through a probe, a thin metal wire.

At first the resonator was rectangular, with outer dimensions of 300x250x100 mm. Later it was studied, what would the effect be on the results, if one of the edges was made slanted, having an angle of 45 degrees. It was known at the time of working on the special assignment [13] in 2008, that many filter presses, to which the resonator might be assembled, do not allow assembling a rectangular resonator. The version of the resonator with the slanted edges was suitable for the application of this thesis as well.

In [13] the resonant frequency, f_r, and the scattering parameter S_{21} were simulated for the cavity resonator using the IE3D electromagnetic field simulator. The f_r and S_{21} with and without the slanted edge were compared. In these simulations, the distance between the resonator halves was first selected to be d = 30 mm and then d = 60 mm while the permittivity of the material was assumed to be $\varepsilon_r = 10 - j$.

It was discovered, that f_r lowers very little, only circa 1 MHz, compared to the rectangular resonator. When the distance is d = 60 mm, f_r lowers a little more, 1.5MHz. In either of the cases (d = 30 mm and d = 60 mm), S_{21} does not change remarkably.

As a conclusion, the change in the outer dimensions of the resonator was shown to have only a slight effect on the resonant frequency. For the resonator that is built to measure the bio material web, all the dimensions are the same as in Figs. 4.1 and 4.2.

The center conductor of the resonator is a butterfly-shaped aluminum strip. The strip determines the measurement area for the resonator. A butterfly-shaped strip is used because the measurement area is much wider than for a narrower, rectangular one [8]. If it is necessary to change the dimensions of the resonator box, it should be avoided on the side where the strip is attached, as in Fig. 4.1.

In [8] the butterfly-shaped center conductor was used in a stripline resonator. Figure 4.3 presents the measurement area of a two-conductor $\lambda/4$ stripline resonator with butterfly-shaped center conductors. The center conductor is 110 mm long and 200 mm long at the wide end. The resonant frequency is 360 MHz and the contour line interval is 15 kHz. The measurement was made by moving a 10-millimeter dielectric sphere in a resonator between the center conductors [8].

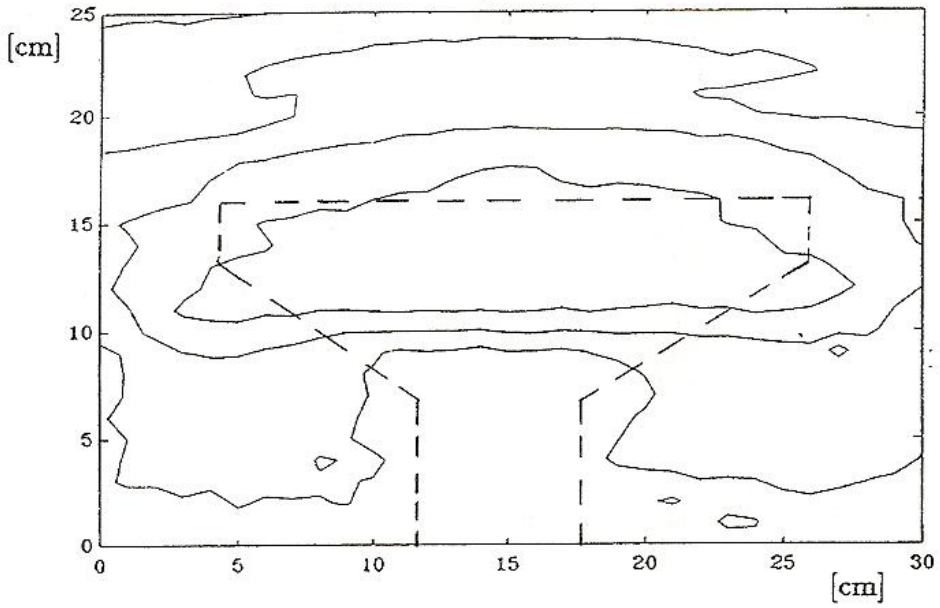

Fig 4.3. Measurement area of a butterfly-shaped center conductor [8].

A prototype resonator was manufactured according to the measures presented in Figs. 4.1 and 4.2. The prototype resonator was built in Protoshop, and it is illustrated in Fig. 4.4. The initial structure had been simulated previously in the special assignment of Tony Niemi and according to the simulations the resonant frequency was 365 MHz [13].

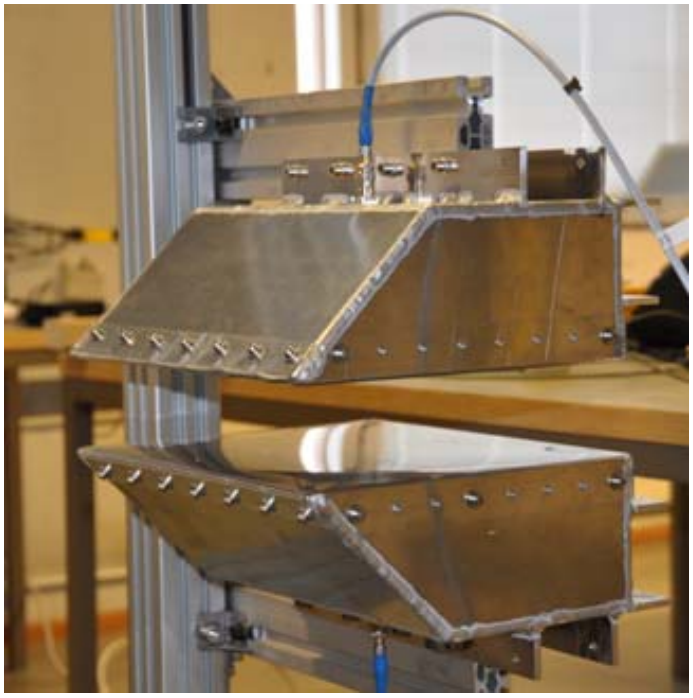

Figure 4.4. The test resonator setup.

The material of the resonator is aluminum. The pieces of the resonator were attached by aluminum welding. The center conductors were attached to the resonator walls with metal screws. This way it is possible to change the height of the center conductors later. This might be needed, if the sensitivity of the resonator is needed to be increased or decreased. In this context the sensitivity means the change of the resonant frequency or the quality factor, when the sample is inserted in the resonator. The vertical dimensions of the resonator affect the sensitivity. If the distance between the resonator halves is increased, the sensitivity decreases. This is because the filling factor decreases; the resonator structure becomes more open [8].

The connectors of the resonator were chosen to be of BNC type because they are known to be quite durable, inexpensive and work well under frequencies of 1 GHz. In the laboratory measurements, however, sma cables were used, as in Fig. 4.4.

The resonator cavities are covered with thin plastic plates in order to prevent the bio material from accumulating in the cavities, especially in on-line usage. The covers are attached to the resonator with metal screws. All these additions to the resonator structure change the performance of the resonator slightly, and affect the resonance curve. The change in the resonant frequency was 0.75 MHz and in the attenuation 0.02dB when the plastic covers were attached. Henceforth, all the measurement results include the effect of the plastic covers.

The vector network analyzer, VNA, which is used throughout the whole work described in this thesis, is the Hewlett Packard (currently Agilent) model HP5753D.

The S_{21} parameter, Fig. 4.5, was measured with a VNA, when the resonator was empty, i.e. without the MUT, but with plastic covers, as shown in Fig. 4.4.

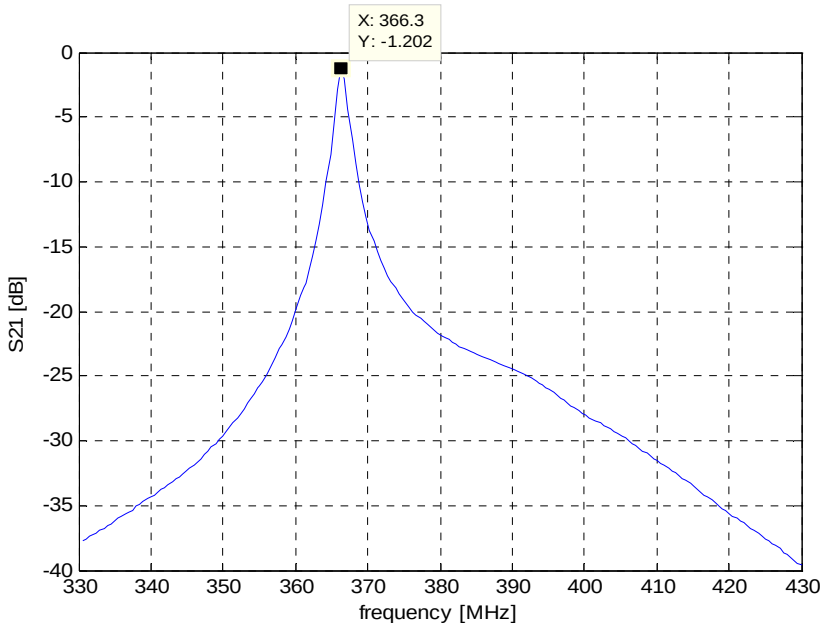

Figure 4.5. S_{21} of the empty (without the MUT) resonator.

The distance of the resonator halves d = 60 mm was measured from the edges of the aluminum. The resonant frequency was found to be 366.3 MHz and the attenuation at the resonant frequency was 1.202 dB. The measured resonant frequency is very close to the simulated f_r that is 365 MHz.

The quality factor can be calculated from the values by using half-power frequencies (Eq. 3.1) [3].

$$Q_l = \frac{f_r}{B_{3dB}} \tag{3.1}$$

By inserting the resonant frequency and the frequencies where the power has dropped 3 dB, the quality factor can be calculated, $Q_l = 203$.

4.2 Testing of the resonator with reference samples

The frequency range of operation of the resonator was defined. For this purpose a reference material sample was prepared. The thickness of the reference material sample should be as close to the average thickness of the bio material as possible.

It is important that the MUT is placed exactly between the resonator halves. The principle of operation of the resonator is such that the more accurately the material is placed just in the middle of the two halves of the resonator structure the more predictable is its operation. For the laboratory measurements a support for the test

sample was developed to place the MUT between the resonator halves. A large Styrofoam plate was placed between the resonator halves. The material was placed on a thin plastic plate so that the material sample could be moved into the resonator on it. Figure 4.6 shows the support and the test sample. With the chosen reference material, cotton, occurred a problem. It thickens when it becomes drier, thus in the last measurements it was remarkably thicker than when the moisture content was 63%. The material was not exactly between the resonator halves and this causes error to the results. However, dry cotton is assumed to be as little electrically visible as the dry material of the bio material web.

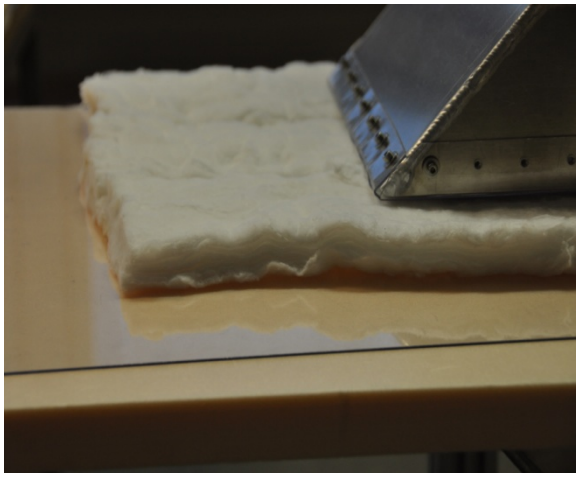

Figure 4.6. Reference material measurement.

It was tested that the Styrofoam and plastic supports are not very visible electrically in the measurement result. Their permittivities are quite low at the frequencies of interest. The effect of the plastic plate on the resonant frequency is -0.4 MHz. The Styrofoam support decreases the resonant frequency 0.1 MHz. Together their effect is thus -0.5 MHz on all the results of the reference material.

The measurement setup of the resonant frequency measurement is presented in Fig. 4.7.

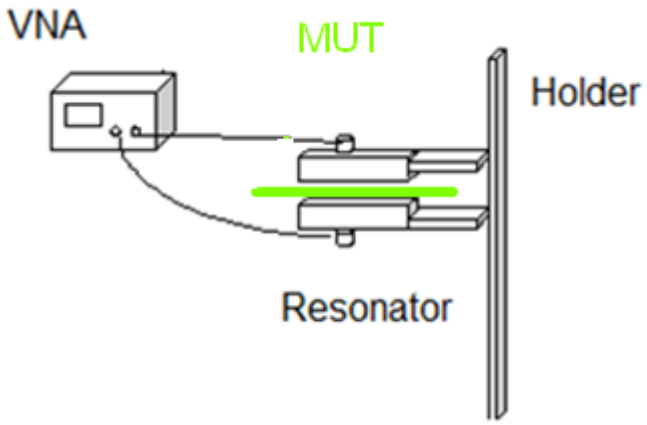

Figure 4.7. Test measurement setup: VNA, resonator , MUT and the holder.

For testing purposes a wet reference material sample was prepared. The idea of the first measurement was to find out how much the resonant frequency decreases compared to the resonant frequency of the empty resonator f_{r0}, when a wet material sample is inserted in the resonator. The frequency range of operation for the resonator can be tested with the reference material.

A cotton sheet was prepared. The thickness was approximately the same as that of the bio material: 13 mm. The initial moisture content of the sample in the first measurement was approximately 60 %. The moisture content was approximately the same as that of the average moisture content of the bio material. The real moisture content could be calculated only after drying the sample.

The liquid that was used to moisten the sample was tap water. The bio material contains also some impurities and salts, i.e. the imaginary part of the relative permittivity can be larger than for tap water. However, with tap water it is possible to measure the maximum resonant frequency shift with rather little effect on the attenuation that can be different or even unpredictable for the bio material. It is assumed that the effect of the imaginary part of the permittivity is rather small. In other words, ε'' is much smaller than ε'.

The resonant frequency decreases when the moisture content increases. The absolute value of S_{21} was measured at different stages of the drying process. In the first measurement of the reference sample, the moisture content was 63% and the resonant frequency was thus at minimum, Fig. 4.8.

The real moisture content of the wet sample could be calculated when the weights of the wettest and oven-dried samples were known. The sample was weighed before measuring to verify the real moisture content. The moisture content calculated from the dry and wet weights is 63%.

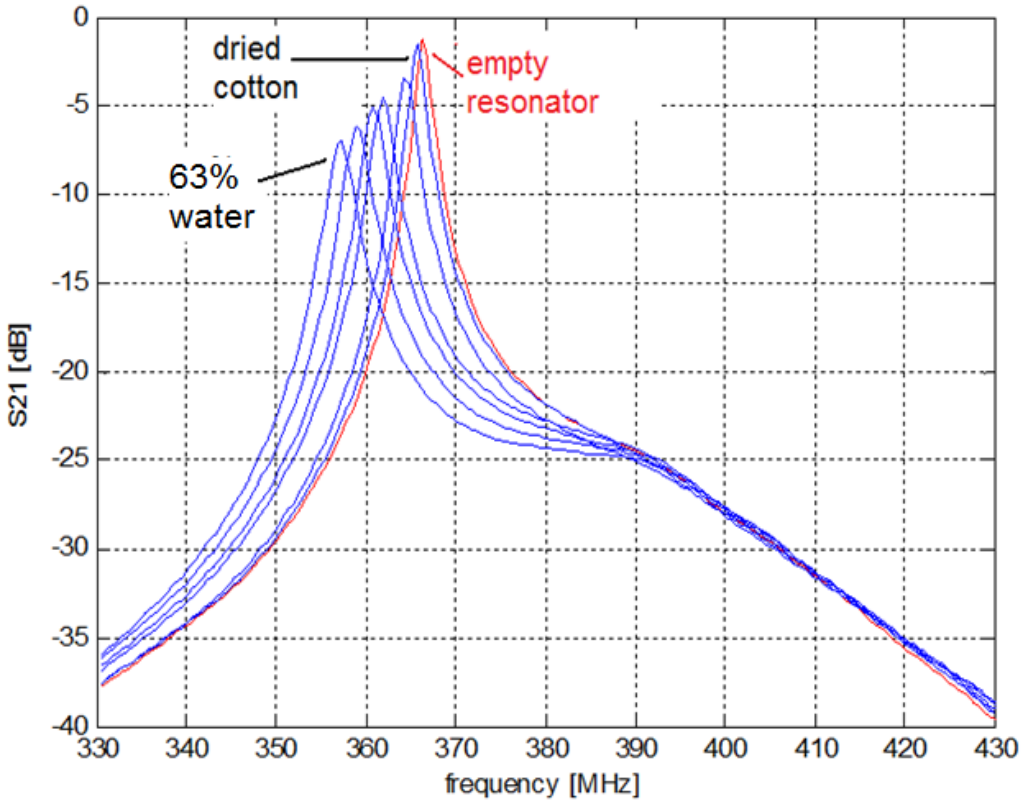

Figure 4.8. The measured resonant frequency with (blue lines) and without (red line) the reference material.

The moisture content of the reference material was calculated from the resonance measurement results (Fig. 4.8). A rule of thumb can be applied for the moisture evaluation: the frequency shift is 150 kHz per one percent unit of moisture. There is an 8.9 MHz decrease in the frequency, when the resonator is filled with the wettest cotton sheet. Based on this approximation, the moisture content of the cotton sheet is thus 59.3%.

The thickness was measured when the cotton sheet was wet. The thickness of the cotton increased during the process of drying. This might cause some error to the results, because in the measurement of the dry cotton, the sheet was not exactly between the resonator halves. The Styrofoam support was designed for the average MUT. However, the dry MUT is not very visible in the results, Fig. 4.8.

4.3 Measuring the bio material with the sensor prototype

The bio material was measured in laboratory conditions in Aalto University, in Otaniemi.

At the time of this measurement some preparations for the factory measurements had already been made. A plastic support for the MUT had been assembled between the resonator halves.

The locations of the center conductors and the sizes of the signal feeding probes were the same as in the measurement of the reference material. Also the SOLT calibration of the VNA was the same.

Bio material samples were sent to Aalto University from the factory. They were wrapped in plastic so that the moisture content would not decrease on the way to the university. Two samples were measured with the resonator. The sizes of the samples were chosen so that the whole measurement area of the resonator would be covered. The samples were approximately 500 mm x 500 mm. The accurate measures are in Table 4.1.

Table 4.1. The areas, weights, thicknesses and initial moisture contents of the bio material samples 1 and 2.

	Surface area	Weight (1) [g]	Weight (2) [g]	Weight (3) [g]	Weight (4) [g]	Weight (5) [g]	Thickness (mean value) [cm]	Moisture content (w.b.) (oven-dried)
Sample 1	480 mm x430mm	2461	2366	1168	1071	1041	1.35	57.7
Sample 2	480 mm x390mm	2478	2253	1485	1026	960	1.375	61.3

The resonant frequency of the resonator without the MUT was measured again, because of the added structures to the resonator, $f_{r0} = 365.8$ MHz.

The samples were measured at different stages of drying. Their moisture contents (%) were calculated by weighing them on a scale and comparing to the dry weight of each sample.

Fig. 4.9 shows the measured S_{21} of the bio material sample 1. Sample 1 was measured at 5 stages of drying, as the moisture content varied from 57.7% to 0%. In Fig. 4.9 there is seen a sudden decrease in the signal level, before it increases again approximately at 395 MHz (black and green lines). This is most likely the odd wave mode of the strip-line resonator. The odd mode is seen, even though the resonator has been designed to support the even mode [13].

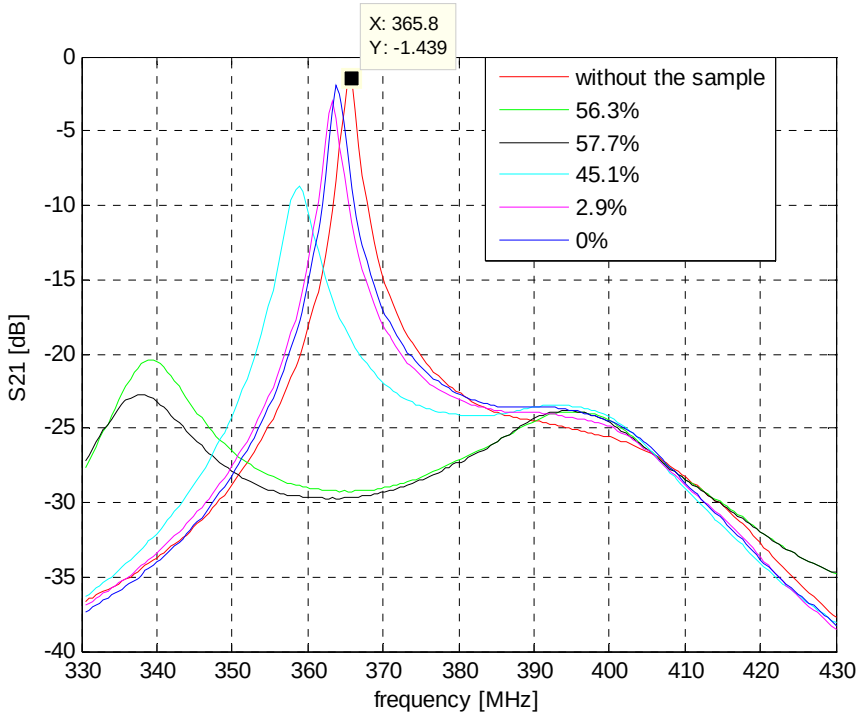

Figure 4.9. The measured S_{21} of the bio material. Sample 1.

Fig. 4.10 presents the S_{21} of sample 2, which was measured at 5 moisture contents: 61.3%, 36%, 22.9%, 7.4% and 0%.

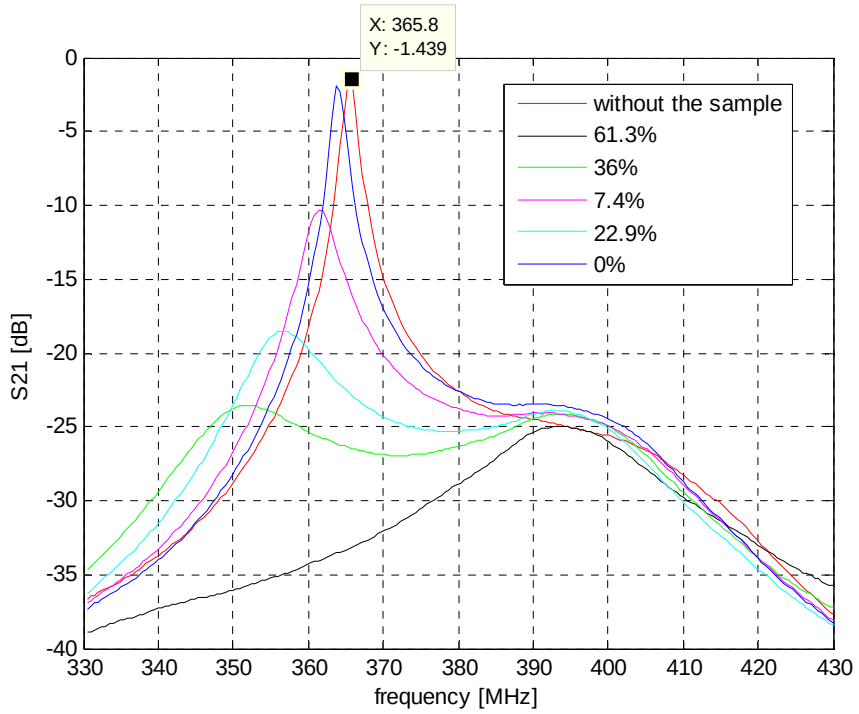

Figure 4.10. The measured S_{21} of the bio material. Sample 2.

By comparing the S_{21} curves of samples 1 and 2, it is seen, that the resonance curves seem quite similar, when the moist MUT is measured. However, sample 2 is obviously more lossy. For sample 1 the level of S_{21} is -22.75 dB and f_r = 338 MHz, when the moisture content is 57.7%, i.e. the moisture that could be in the factory circumstances. For sample 2, S_{21} = -23.56 dB, f_r = 351.9 MHz and there is 36% water. When the moisture content of sample 2 is 61.3%, no resonant frequency can be defined.

From this laboratory measurement one achieves information on, what is the frequency range over which the resonant frequency changes, when the bio material is measured. Also, it is important to test the attenuation of the signal with the bio material; if the material behaves alike sample 2, the factory measurement might not become successful. However, based on this laboratory measurement, the prototype resonator is not changed in any way due to lack of time.

Relative moisture contents (% of weight) were used as reference moisture contents. This is sufficient to define the suitability of the resonator for the bio material, even though it is not possible to define the relative moisture content of the MUT with the resonator.

From these two samples it would be impossible to find a calibration for the resonator. It is not possible to predict the behavior of the bio material based on this laboratory measurement. Therefore, the calibration and defining the moisture content based on the resonance measurement, is made in Sec. 4.4.3. Instead, the frequency range over which the factory measurements are performed is chosen to be from 310 MHz to 380 MHz.

4.4 Factory tests

4.4.1 Measurement setup

The measurement setup in the factory measurements is illustrated in Fig. 4.11. The setup consists of the resonator sensor assembled to the belt filter press, a VNA, and a laptop. The measuring device is connected to the laptop with a Prologix GBIP to USB controller cable [14]. The VNA that is used in the factory measurements is the same as in the laboratory measurements.

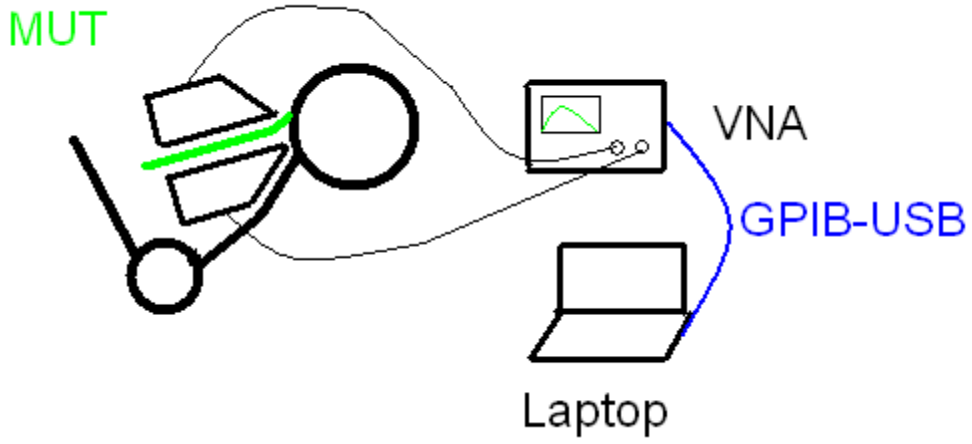

Fig. 4.11. The measurement setup in the factory measurements.

One issue of the measurement system is the measurement time. The speed of the conveyor belt, approximately 1 m/min (verified from the paper factory), affects the requirement for measurement time. It is tolerable if the belt moves at maximum 10 mm during the measurement. Since the speed of the belt is so low, only 16.7 mm/s, it is estimated that measuring over the entire frequency range should not take more than approximately 590 ms. B.Sc. Jan Järveläinen has programmed a control system for the VNA to measure 51 points over the frequency range from 310 MHz to 380 MHz that is used in the measurements. A control system is built to measure the S_{21} at the desired frequency points. The frequency range was evaluated in the laboratory measurements. The measurement time with the developed control system is 25 ms, which is clearly sufficiently low. The program that controls the VNA is run from a laptop. The results are saved in ASCII form to the hard drive of the laptop.

When the resonator was designed, the known average thickness of the MUT, i.e., the bio material web was d_{ave} = 13 mm. The space between the resonator halves was chosen *d* = 60 mm based on previous simulations [13]. Taking into account the perturbation theory of the even wave mode, support structures were attached to the resonator to direct the MUT to slide exactly between the resonator halves. Figure 4.12 shows the dimensions *d1* to *d8* of the measurement setup. The average thickness of the bio material is denoted with *d4* = d_{ave}. The support structure that holds the support '*d3*', is *d6* = 17 mm measured from the aluminum edge of the resonator. The space between the resonator halves was set to *d* = *d5* = 60 mm. If the thickness of the MUT varies remarkably, the bio material web will not be exactly between the resonator halves, which causes error. In the factory measurements it was not possible to set the MUT exactly between the resonator halves with the accuracy of millimeters.

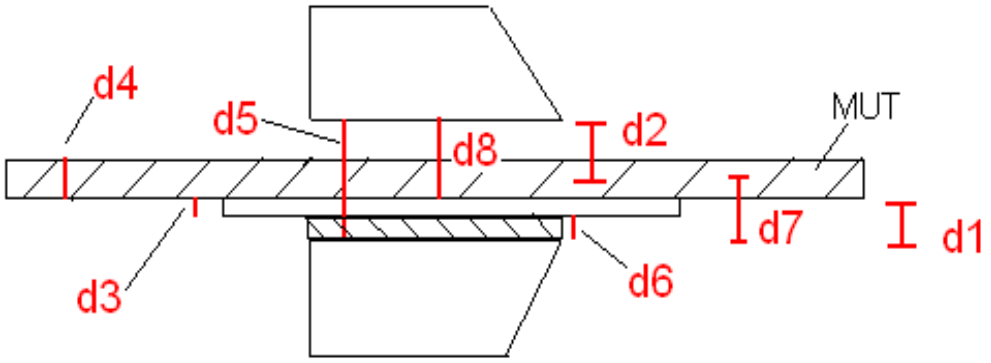

(a)

d	**[mm]**
d1	22
d2	31.5
d3	5
d4	13
d5	60
d6	17
d7	28.5
d8	38

(b)

Figure 4.12. The dimensions *d1* - *d8* of the sensor in the factory measurements. The position with respect to the sensor **(a)**. Table for measures *d1* to *d8* **(b)**.

To measure in online conditions, the prototype resonator was assembled to the filter press according to Fig. 4.13. The lower and upper halves of the resonator were attached to the filter press. The upper half was connected with 60 mm adjustable profiles which made it possible to move the upper resonator half upwards or downwards in order to set the space between the halves to *d* = 60 mm as it was in the laboratory measurements.

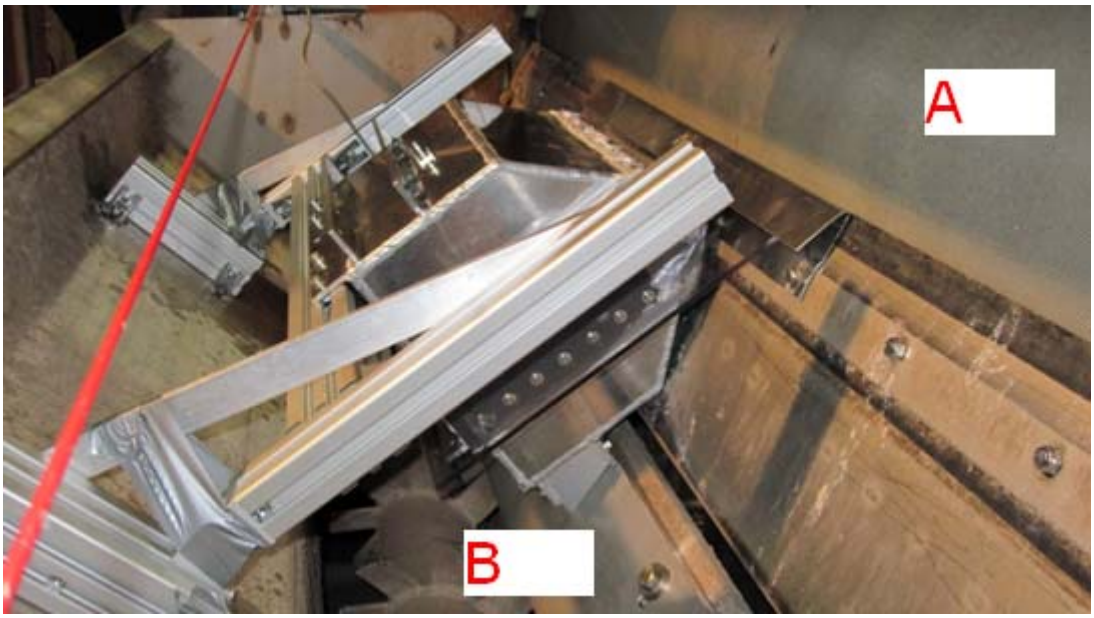

Figure 4.13. The resonator halves assembled to the filter press.

In Fig. 4.13 the bio material web is still not flowing through the halves. The plastic support of size 550 mm x 340 mm is meant to direct the MUT in such a way that the MUT, while moving through the resonator, is positioned exactly between the resonator halves. The bent metal plate is used to direct the MUT above the plastic support. The area that is denoted with letter A is the belt on which the bio material web is brought to the cutter (denoted with the letter B). From the cutter, the shreds of the bio material are dropped to a conveyor belt and moved to a container and later moved to be burnt.

Figure 4.14. The bio material web flows between the resonator halves.

In Fig. 4.14 the bio material flows through the resonator. It can be seen that the MUT stays intact during the measurement in the measurement area, between the resonator halves.

4.4.2 Resonator sensor measurements of MUT and collecting of reference samples

In this section the results from the resonator sensor measurement are described. The measurements were performed in the factory during two days. During this time, in total 97 reference samples were manually collected and 97 measurements with the resonance sensor system were simultaneously performed and saved to a text file. The samples were taken a bit above the measurement area of the resonator, because it was necessary considering labor safety. The area of which the samples were taken is the part of the web before it flows into the resonator, as shown in Fig. 4.14.

Fig. 4.15 presents all the 97 resonant curves (black) and the resonance curve of the resonator without the MUT (red). Already at this point, it became obvious that there are deviations among the measured samples.

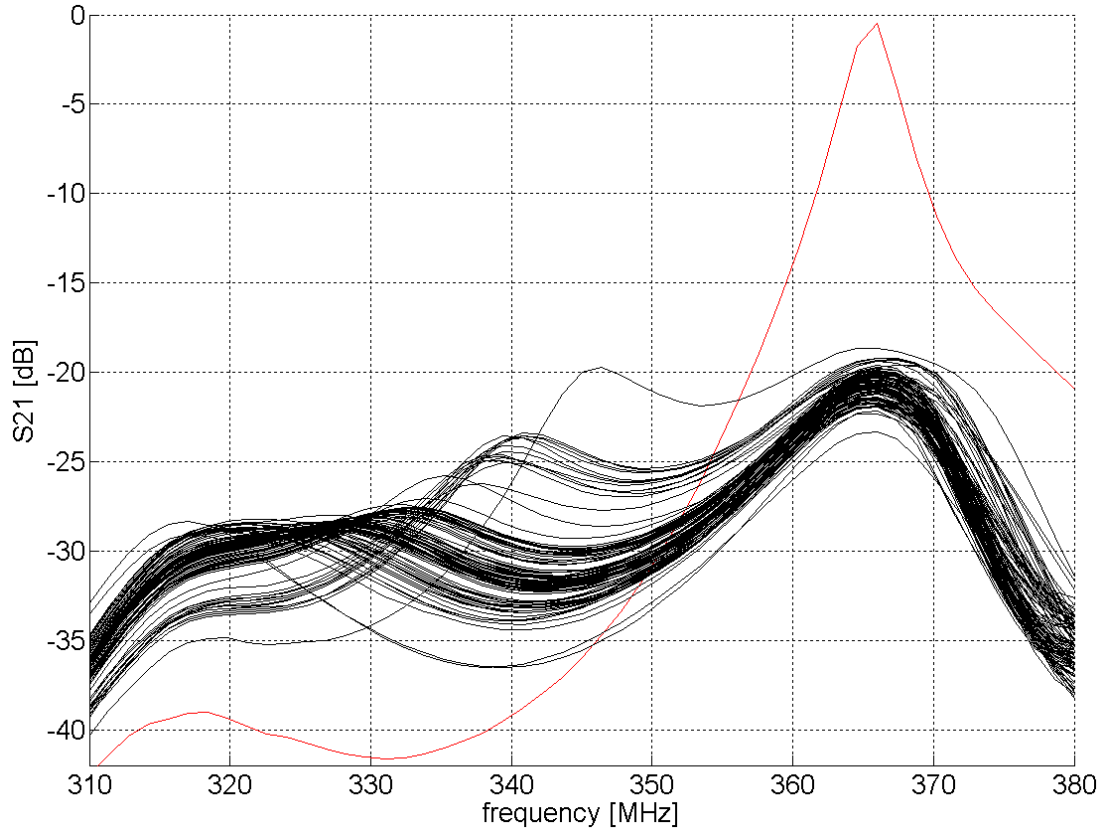

Figure 4.15. The 97 resonance curves with the bio material inside the resonator (black lines) and the resonance curve of the empty resonator (red line).

The measurements were performed in such a way that a set of 8 to 10 measurements were conducted at a time within a relatively short period of time (approximately 10 to 20 minutes) after which the corresponding set of 8 to 10 reference samples were collected manually. The resonance curves for the different sets of measurements are presented in Figs. A.1 to A.12 in App. A.

The resonant frequencies of the samples are found with a Matlab algorithm and the frequencies as well as the corresponding attenuations of the resonance curves are listed in Table A.1 in App. A. The resonant frequency of the resonator without the MUT was measured before turning on the process when the material did not flow through the resonator yet. The resonant frequency was $f_{r0} = 366$ MHz.

The measurement conditions in an online measurement differ from those of laboratory conditions. In the laboratory measurement the MUT was placed between the resonator halves. The resonance curve on the screen of the VNA was thus stable. In an online measurement the MUT moves e.g. on a conveyor belt at a certain speed. The structure and the water content are uneven at different spots of the MUT. When this kind of uneven material moves between the resonator halves, the resonant frequency and attenuation of the resonance curve change constantly. When the measurement is done with a VNA, the shape of the resonance curve might have changed before the points of interest are read to a text file.

The method of defining the moisture content that is used is by calculating the amount of water in grams per the whole mass of the sample. This is the method that has been used in the factory to define the moisture content of the bio material web. The resonance measurement is, however, based on measuring the change in the resonant frequency which is proportional to the amount of water per surface area of the bio material. The method of analyzing the water content with the resonator is discussed in detail in Sec. 4.4.3.

Table B.1 shows the reference moisture contents of the 97 samples that were analyzed in the laboratory of the paper factory. The average moisture content is 56.4 % and the standard deviation σ = 1.35 % units.

The thicknesses of all 97 samples are listed in Table B.3. The average of the thicknesses is 12.24 mm and the standard deviation σ = 2.22. The average thickness is close to the earlier estimated average thickness d_{ave} = 13 mm on which the design of the resonator was based. The thickness of the MUT varies from 7 mm to 21.4 mm. The thicknesses of samples 65 to 96 were measured in the factory. This causes some error, because the samples were not measured with the same caliper. The error is studied in detail in Sec. 4.5.2.

In addition to the 97 samples that were dried in the factory, 64 samples of the MUT were brought to Aalto University in order to define their volumes. The moisture contents of these samples were measured, and they are listed in Table B.2. The average

of the moisture contents that were measured in Aalto University is 57.6 % and the standard deviation σ = 1.56 % units.

The samples that were dried in the factory and in Aalto University were taken from the same manually collected samples, so the reference moisture contents are related to the same resonant measurements as those that are dried in Aalto.

4.4.3 Measurement results and analysis

In this section the results of the sensor measurements are analyzed. The main results of this thesis are presented. Based on the perturbation theory for the stripline resonator that has been used, it is estimated that when $\varepsilon_r'' \ll \varepsilon_r'$, the change in the resonant frequency due to the MUT is linearly dependent on the amount of water in the MUT. Thus, the relative resonant frequencies as a function of the amount of water are fitted to a line in Subsection 4.4.3.3.

The amount of water in each of the taken samples is expressed as the thickness of the equivalent water layer. The concept is clarified in Sec. 4.4.3.2 and it is also described how the equivalent water layer is defined.

4.4.3.1 Deriving the linear dependency from the perturbation theory

Based on the perturbation theory (Sec. 3.3.1), it is possible to make an analysis on the resonance measurement results. An assumption is made for the bio material that $\varepsilon_r'' \ll \varepsilon_r'$. It is also assumed, that the imaginary part might change quite a lot depending on the consistency of the waste water. Therefore, only the real part of the relative permittivity ε_r' can be used to deduce the results from the measurements. For the even mode, the change of the resonant frequency linearly depends on ε_r', Eq. (3.9). Since it is assumed that $\varepsilon_r' \gg 1$, Eq. (3.9) comes to the following form

$$\frac{\Delta f_r}{f_r} \approx -\frac{\varepsilon_r'}{2} \cdot S \tag{4.1}$$

The filling factor S can be solved from the data that has been achieved from the reference moisture content measurement and the resonance curve measurement.

4.4.3.2 Determination of the thickness of the equivalent water layer

Under the assumptions made in Sec. 4.4.3.1, the resonator that is used for measuring the moisture content of the bio material layer detects the amount of water that is between the resonator halves at the moment of the measurement.

To make an analysis on how the resonant curve changes, when the moist MUT is placed in the resonator, it is necessary to know the amount of water in the samples per volume. Since the areas of both the water layer and the whole MUT are the same, it is

sufficient to know the thicknesses of the samples and the amount of water in them to make the analysis.

The water contents of the samples 0 to 64 are known in grams. The assumption is made that anything that has evaporated from the sample is pure water. The density of water is 1 kg/dm^3. The volume of the sample is known because its area and thickness were measured. The equivalent water layers of the samples are calculated by dividing the volume of the water by the area of each sample. The equivalent water layers, h_w, are listed in Table B.4.

4.4.3.3 Results

In Fig. 4.16 the relative change in the resonant frequency, $\Delta f_r/f_r$, of the samples are presented as a function of the equivalent water layer h_w. The samples are fitted to a line (4.2) by calculating the average of the slopes that are calculated for each sample by $(\Delta f_r/f_r)/h_w$. The values are listed in Table B.4.

$$y = 0.01515x \tag{4.2}$$

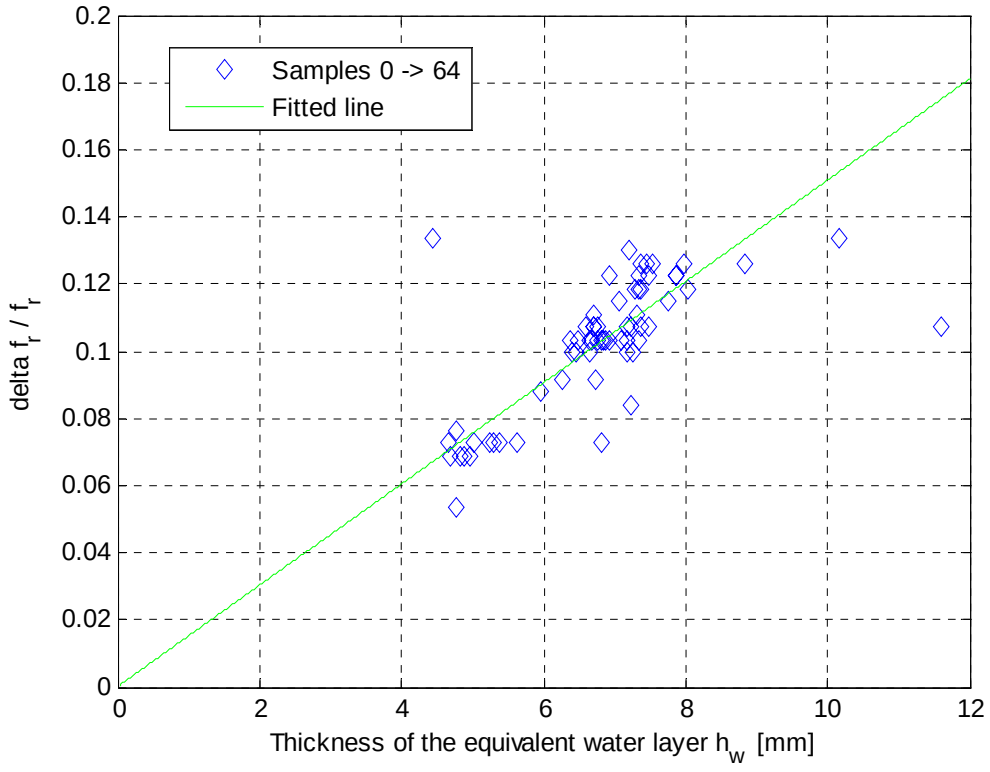

Figure 4.16. The relative change in the resonant frequency as a function of the equivalent thickness of the water layer (sample numbers from 0 to number 64).

The error of $\Delta f_r/f_r$ is calculated for the matching of the samples. The standard deviation from the fitted line (4.2) is 0.01497.

When the resonator was designed, the known value for the average thickness of the bio material web was d_{ave} = 13 mm. The thickness of the MUT, however, varies from 7 mm to 21.4 mm. The resonator might not function as wanted if the thickness of the MUT is much larger or smaller than d_{ave}. Therefore, a thickness-compensated frequency response needs to be evaluated, (Sec. 4.4.4).

4.4.4 Results after removal of too thick and too thin samples from analysis

If the MUT is remarkably thicker than d_{ave}, the linear dependency between the $\Delta f_r/f_r$ and the equivalent water layer, h_w, will not apply. Therefore, in this section the standard deviation of the thickness of the MUT is studied, and the deviant samples are removed from further analysis. The remaining samples are fitted to a line.

The standard deviation of the thickness based on samples 0 to 96 is σ = 2.22 mm, calculated from the values of Table B.3. The samples are analyzed based on how far (how many standard deviations, σ) they are from the average thickness, d_{ave} = 13 mm, that the design of the resonator was based on.

The value 1.5σ equals to 3.33 mm. Thicknesses that deviate less than 1.5σ from the average are allowed. Hence, the samples with thicknesses over 16.33 mm or less than 9.66 mm have to be ruled out from the following analysis. The samples that are left out are numbers 1, 2, 4, 5, 6, 9 and 33 to 40. The samples 1 and 2 are over 20 mm, and this might be because the process had not stabilized yet. The first samples were taken quite soon after the process of the filter press had been started. On the contrary, the samples 33 to 40 are too thin. The thicknesses of these samples were measured in Aalto University and they might have dried during the transportation. This could make the samples thinner.

In Fig. 4.17 the relative change in the resonant frequency, $\Delta f_r/f_r$, as a function of the thickness of the equivalent water layer is presented for the remaining samples.

With the samples that fit to the limit of less than 1.5σ, a thickness-compensated fitting to a line can be made. The line (4.3) that fits to the remaining samples, is achieved by calculating the average of the slopes achieved from the measurement data, that are listed in Table B.5

$$y = 0.015177x\,. \tag{4.3}$$

The samples' standard deviation of $\Delta f_r/f_r$ from the line is 0.0133.

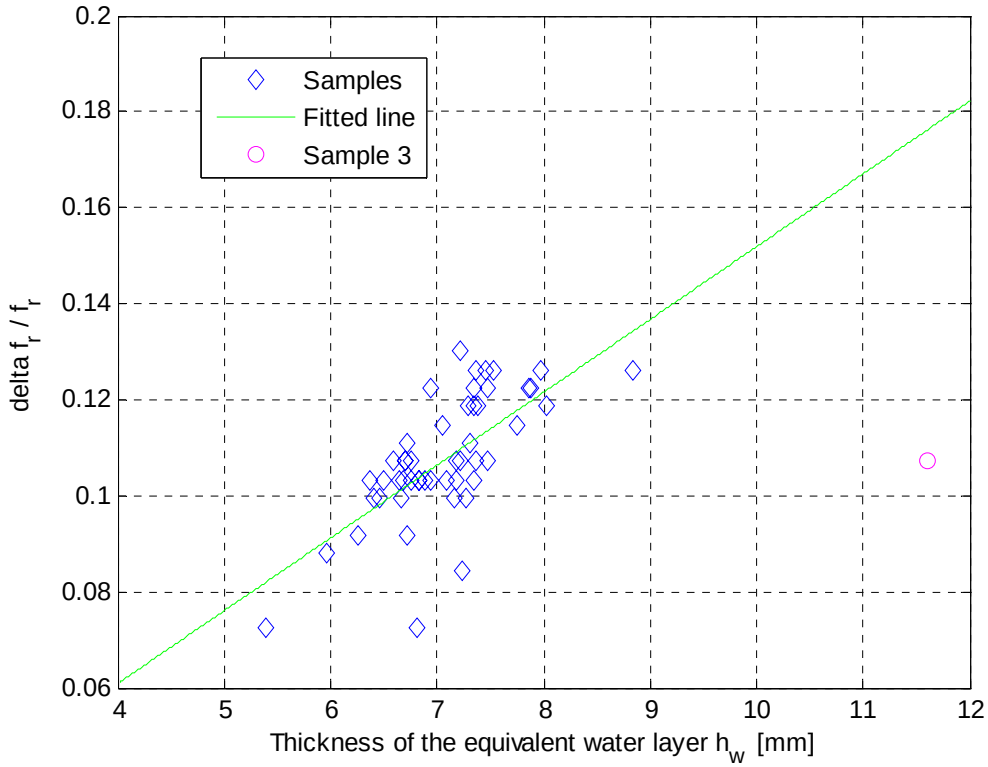

Figure 4.17. The relative change in the resonant frequency as a function of the equivalent thickness of the water layer.

Obviously, sample 3, which is marked with red, does not match the other data in Fig. 4.17. Sample 3 causes error to the slope of the line (4.3). However, its thickness is only 14.37 mm so it fits to the standard deviation limit 1.5σ of the thickness. The problem with the sample is that the sample has too small a change in the resonant frequency compared to the large equivalent layer of water: 11.60 mm. The error that is caused might be because also the other samples from the beginning of the process did not match the average. Or quite simply the material sample might be such, that it is not possible to measure its moisture content with the resonance measurement.

4.5 Uncertainty analysis

The defining of the resonant frequency might be difficult the larger the permittivity of the MUT becomes. The permittivity increases for the bio material if the height of the equivalent water layer increases. The effect of the MUT can be seen from the resonance curves (Figs. A.1 to A.12). When the permittivity increases, the resonance curve becomes wider, thus it might be harder to define the resonant frequency of the resonance peak. All kinds of losses in the material can affect especially the attenuation of the resonance peak. In the laboratory measurements of the bio material it was seen,

that the material might behave surprisingly; the attenuation might be larger even if the relative moisture content of the material is approximately the same as that of some other sample taken from the bio material web. The resonance curve might be lost among the noise, this means that the resonance peak is so low that it is hard to find the f_r by any algorithm. Therefore, it was verified from Figs. A.1 to A.12 that the right resonant frequencies had been found with the Matlab algorithm.

4.5.1 Calibration of the resonator

The conditions are rarely absolutely stable in a factory. The temperature can change many degrees between day and night. Therefore, the calibration has to be done again at fixed intervals; the resonant frequency of the resonator without the material needs to be measured often enough.

The changes in the temperature affect the resonant frequency through the thermal expansion of aluminum: the dimensions of the resonator change. In the factory measurements a thermometer is thus needed. If the temperature changes remarkably in the factory, it might be necessary to take into account the change in the permittivity of water due to variations in the temperature (Sec. 2.2).

These additions to the measurement system might require some changes to the control system's algorithm.

4.5.2 Reference measurement of the thickness

The samples from number 0 to number 64 were measured in Aalto (both the thickness and the moisture content by the oven-drying method). Since the thicknesses of the rest of the samples (from number 65 to 96) were measured in the factory, it was tested, how much is the effect of the caliper, which is used. Also, the sample might dry during the transportation. Four additional test samples were taken and measured in the factory and in Aalto University, and the thicknesses of these samples are listed in Table 4.2. Three values were measured because the thickness can vary even within a small 100 mm x 100 mm sample. Their averages [mm] are shown in table B.3.

Table 4.2. The thicknesses of four test samples.

Sample	Thickness [mm] (in the factory)	Thickness [mm] (in Aalto University)
1	12,64667	13,8
2	12,24667	13,167
3	12,44333	12,5
4	12,03667	13,5

The assumption was that the thickness should reduce during transportation from the factory to Aalto University because the samples would dry. From Table 4.2 it is obvious,

that the measurement inaccuracy of the caliper affects more than the drying. The thickness seems to have increased rather than decreased.

4.5.3 Sensitivity of the resonator sensor

If the level of the signal attenuates close to the noise level, the signal might not be detected properly. As it can be seen from the laboratory measurements of the bio material web, Figs. 4.9 and 4.10, the level of the resonance peak becomes too low for the wettest sample: below -20dB for sample 1 and below -35dB for sample 2.

Thus, the sensitivity of the resonator might have to be modified later during the process of development of the resonator sensor system. This is, however, outside the scope of this thesis.

CHAPTER 5

CONCLUSION

In this thesis, moisture measurement of a biomaterial using a resonator sensor has been studied. The resonator-based RF moisture measurement has been previously used for plywood. The purpose was to study, whether the method of moisture measurement is applicable to the bio material web. A known resonator structure, a strip-line cavity resonator was chosen to be the sensor. It was especially studied, whether the chosen structure can be used in the moisture measurement.

The designing of the sensor was based on the known average thickness of the MUT, namely 13 mm. The operation of the resonator was tested with a reference material. The frequency range of the resonator was tested when the reference material had a moisture content of approximately that of the bio material.

It was also verified in the laboratory of Aalto University that the resonator would function when two bio material samples were measured. The resonance curves were measured for different relative moisture contents. The most important result is the resonance curve for the wettest situation, i.e. that of the MUT in factory measurements. The resonance peak could be detected for the other one of the samples, whereas for the other the level of the signal was -35dB. This indicates, as assumed earlier, that the bio material samples that are taken randomly of the belt filter press are rather inhomogeneous. The bio material is also very lossy.

Measurements were made in the paper factory. The equivalent water layers of 65 reference samples were defined and compared to the resonance curve measurement results. It was estimated, that the dependency between the relative resonant frequency shift caused by the MUT is linear as a function of permittivity. Thus, the samples were fitted to a line. The standard deviation of the relative resonant frequency shift was found to be 0.01497, when all the samples were taken into account. When the samples with thicknesses less or over 1.5σ were ruled out form the analysis, the standard deviation of the relative resonant frequency shift decreased to 0.0133.

5.1 Future work

The strip-line cavity resonator was not modified before measurements of this thesis. The levels of attenuation when measuring the bio material might be too low for the resonator that was used.

In the factory measurements it was noticed, that the bio material varies a lot in thickness. Even the relative moisture content varies between the samples. Therefore, in the future measurements, a much larger amount of samples needs to be analyzed. Although the number of samples taken in this thesis for the analysis was quite small, namely 65, the results hint that controlling of thickness of the bio material is important.

A thickness sensor is necessary to control the changes in the thickness of the MUT. Namely, the flow of water through the resonator depends on the thickness of the bio material layer. The resonator that has been presented in this thesis measures only the water layer between the resonator halves.

As to the mechanical implementation of the resonator setup, there were some disadvantages. In order to use the designed resonator sensor as a part of the process of the belt filter press, some modifications should be made. For online measurement the space of 60 mm between the resonator halves could be too small. In the factory measurement, that are described in Sec. 4.4 it was noticed that when the resonator measurement is on-going, the resonator cannot be left unsupervised. The bio material web started accumulating between the resonator halves at times.

REFERENCES

[1] A. Lehto and A. Räisänen, *RF- ja mikroaaltotekniikka* (in Finnish, RF and microwave technology)*, 8th ed.*, Oy Yliopistokustannus/ Otatieto, 1994

[2] D. M. Pozar, *Microwave engineering, 2nd ed.*, John Wiley & Sons, Inc., 1998

[3] A. V. Räisänen and A. Lehto, *Radio Engineering for Wireless Communication and Sensor Applications,* Artech House, Inc., 2003

[4] A. Sihvola and I. Lindell, *Sähkömagneettinen kenttäteoria 2. Dynaamiset kentät* (in Finnish, Electromagnetic field theory, dynamic fields)*, 3rd ed.*, Oy Yliopistokustannus/Otatieto, 1996

[5] E. Nyfors and P. Vainikainen, *Industrial microwave sensors*, 1989

[6] S. Okamura, "Microwave Technology for Moisture Measurement," pp. 205-227, Plenum Publishing Corporation, 2000

[7] A. Kraszewski, "Microwave aquametry: An Effective Tool for Nondestructive Moisture Sensing," pp. 347-362, 2001

[8] M. Fischer, P. Vainikainen, and E. Nyfors, "Design Aspects of Stripline Resonator Sensors for Industrial Applications," *Helsinki University of Technology Report S214*, ISBN 951-22-2710-X, 1995

[9] A. Kraszewski, *Microwave aquametry, Electromagnetic wave interaction with water-containing materials*, IEEE Press, 1996

[10] M. Fischer, P. Vainikainen, and E. Nyfors, "Dual-mode stripline resonator array for fast error compensated moisture mapping of paper web", pp. 1133-1136, 1990

[11] E. G. Nyfors, "Cylindrical microwave resonator sensors for measuring materials under flow," *Helsinki University of Technology Report S243*, 2000

[12] L. Chen and V. K. Varadan, *Microwave electronics: measurement and materials characterization*, John Wiley and sons Ltd., 2004

[13] Tony Niemi, "Onteloresonaattorin simulointi (in Finnish)," *a special assignment*, 2008

[14] Prologix GPIB-USB Controller webpage
http://www.prologix.biz/

APPENDIX A

MEASUREMENT RESULTS

A.1 Resonant frequencies and attenuations

Table A.1. The resonant frequencies and attenuations of the samples 0 to 96.

Sample	f_r [MHz]	Amplitude (dB)
0	339.4000	-24.7748
1	317.0000	-28.3322
2	317.0000	-29.0742
3	326.8000	-28.0063
4	338.0000	-26.2547
5	339.4000	-23.5753
6	340.8000	-23.3935
7	328.2000	-28.3288
8	339.4000	-24.9512
9	346.4000	-19.7369
10	328.2000	-28.6127
11	328.2000	-28.5064
12	326.8000	-28.7778
13	328.2000	-28.3566
14	324.0000	-29.1194
15	319.8000	-28.8894
16	318.4000	-28.8600
17	319.8000	-28.5174
18	319.8000	-28.8624
19	322.6000	-28.7392
20	322.6000	-28.8037
21	324.0000	-28.9788
22	325.4000	-28.7869
23	326.8000	-28.4989
24	335.2000	-25.7855
25	328.2000	-28.7488
26	326.8000	-28.5700
27	328.2000	-28.8393
28	325.4000	-28.9224
29	329.6000	-28.5616

30	329.6000	-28.5268
31	328.2000	-28.8160
32	328.2000	-28.6188
33	340.8000	-23.5598
34	340.8000	-23.5424
35	339.4000	-24.4288
36	339.4000	-24.0882
37	339.4000	-24.6405
38	339.4000	-24.7400
39	339.4000	-25.0799
40	340.8000	-23.6724
41	333.8000	-27.0687
42	332.4000	-27.5857
43	332.4000	-27.7165
44	329.6000	-28.2249
45	328.2000	-28.3220
46	326.8000	-28.6424
47	326.8000	-28.8453
48	326.8000	-28.7873
49	321.2000	-28.3971
50	322.6000	-28.4635
51	319.8000	-28.7859
52	321.2000	-28.7037
53	319.8000	-28.7592
54	322.6000	-28.2091
55	321.2000	-28.4543
56	321.2000	-28.4994
57	326.8000	-28.4627
58	321.2000	-28.7425
59	328.2000	-28.4277
60	328.2000	-28.4036
61	326.8000	-28.3344
62	328.2000	-28.4624
63	329.6000	-28.0392
64	329.6000	-28.1320
65	332.4000	-27.5727
66	332.4000	-27.7558
67	332.4000	-28.1222
68	332.4000	-27.6092
69	332.4000	-27.6134
70	332.4000	-27.7503
71	333.8000	-27.5594
72	331.0000	-27.9300
73	332.4000	-27.5770
74	331.0000	-27.7264
75	332.4000	-27.5996
76	331.0000	-27.8568
77	332.4000	-27.7805
78	332.4000	-27.6959
79	331.0000	-28.0293
80	332.4000	-27.8720
81	332.4000	-27.3969

82	331.0000	-28.0626
83	331.0000	-28.0411
84	329.6000	-28.2969
85	329.6000	-28.3707
86	329.6000	-28.7562
87	328.2000	-28.5627
88	328.2000	-28.5234
89	329.6000	-28.4135
90	328.2000	-28.4935
91	326.8000	-28.8070
92	326.8000	-28.6372
93	326.8000	-28.6458
94	328.2000	-28.4448
95	328.2000	-28.5162
96	329.6000	-28.6404

A.2 Resonance curves

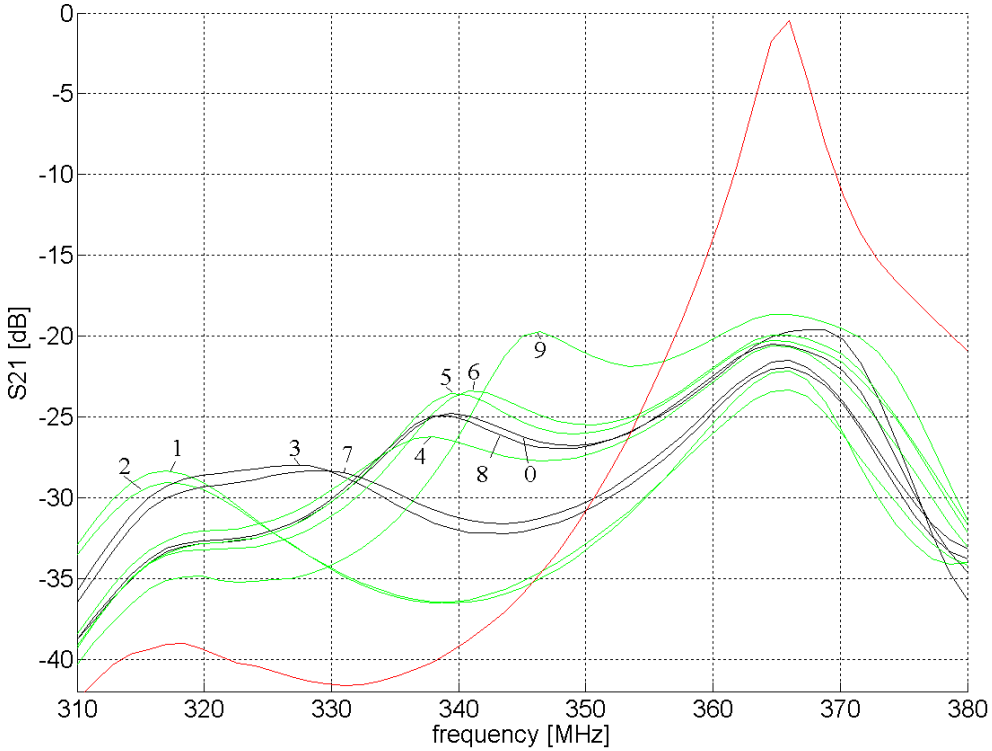

Figure A.1. Resonance curves and the corresponding sample numbers 0-9.

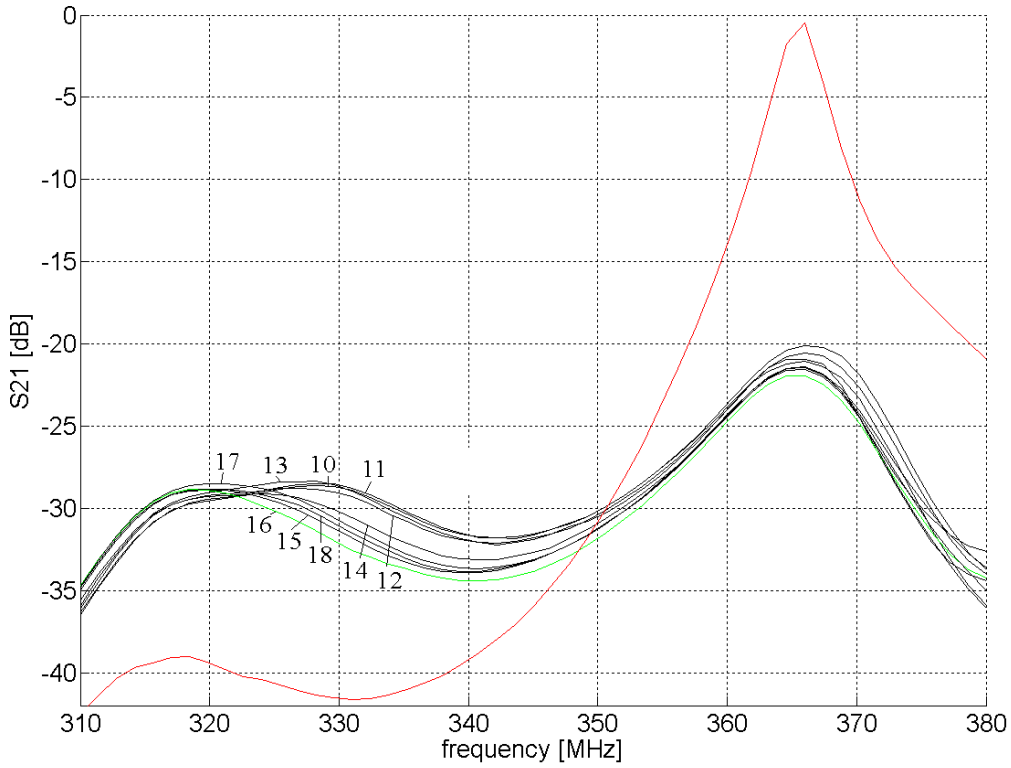

Figure A.2 Resonance curves and the corresponding sample numbers 10-18.

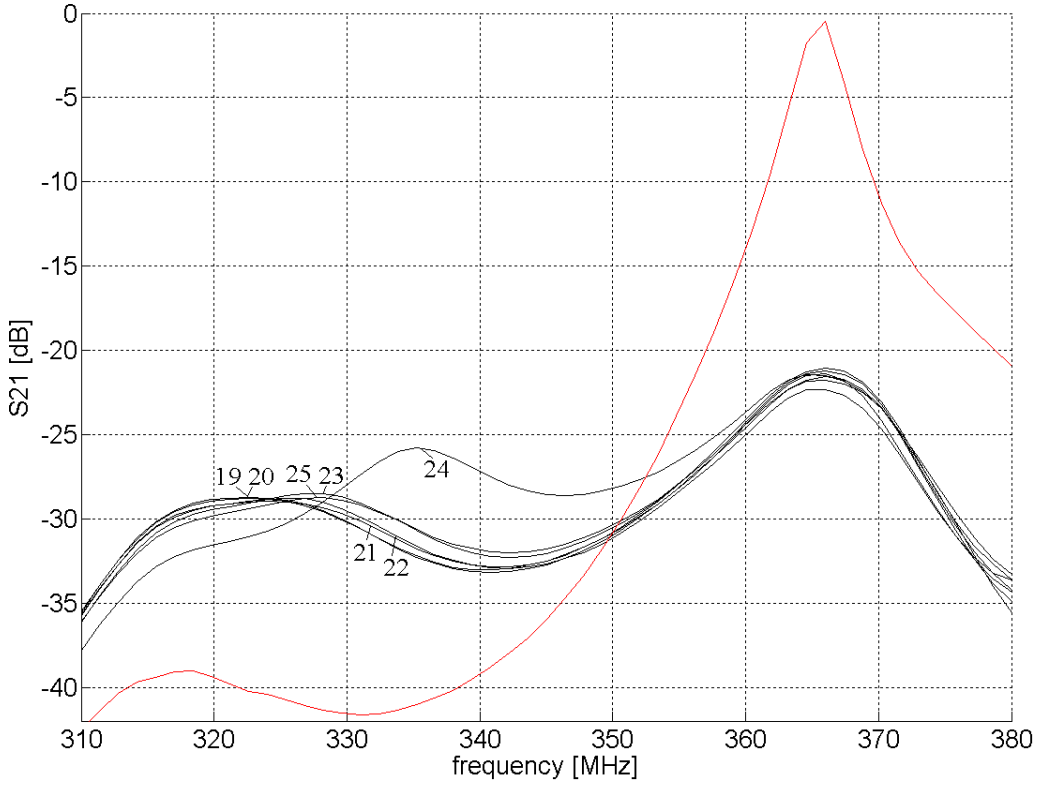

Figure A.3. Resonance curves and the corresponding sample numbers 19-25.

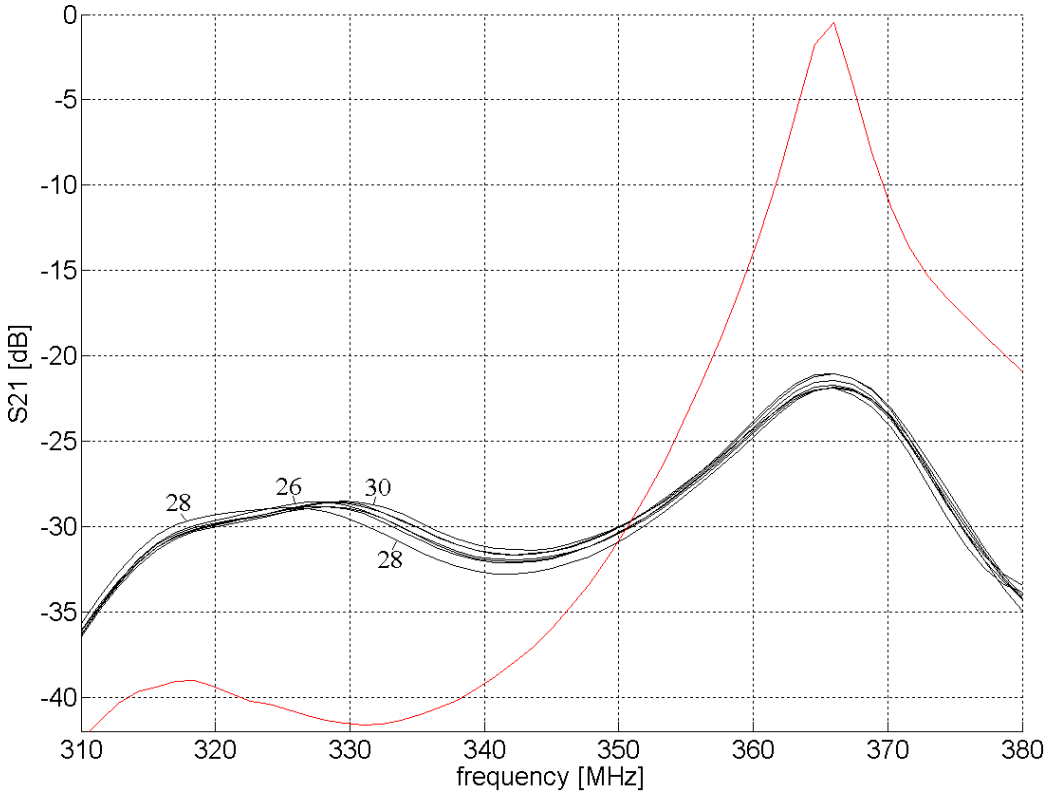

Figure A.4. Resonance curves and the corresponding sample numbers 26-32.

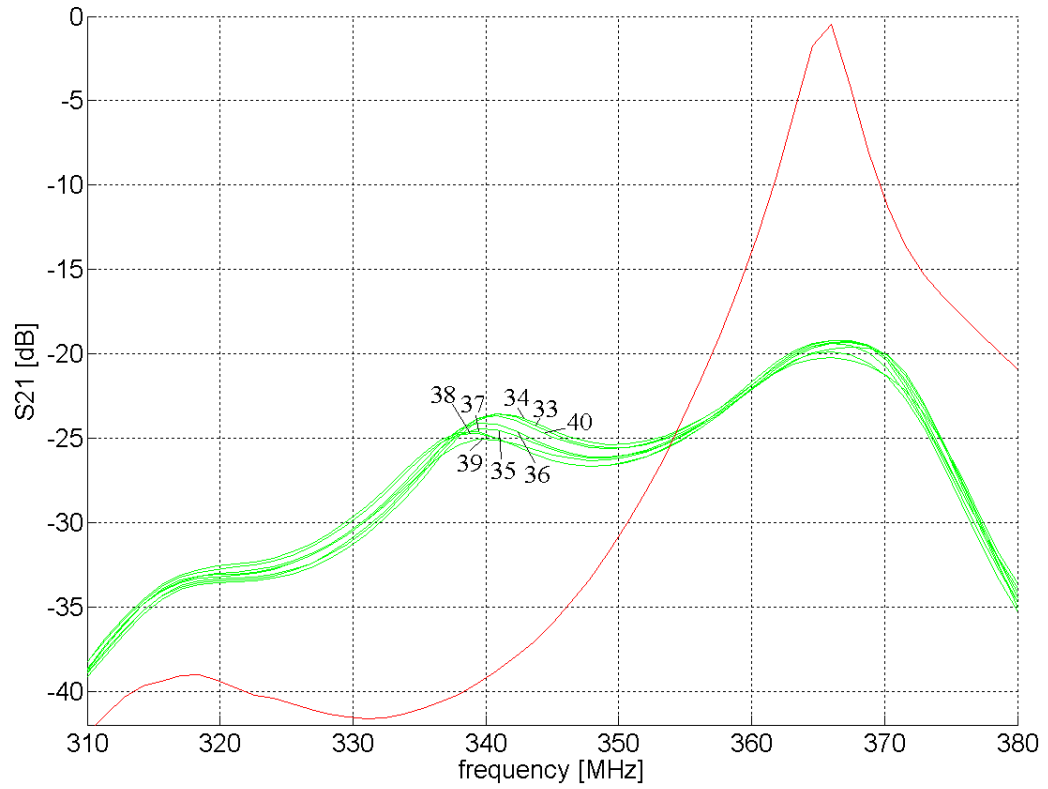

Figure A.5. Resonance curves and the corresponding sample numbers 33-40.

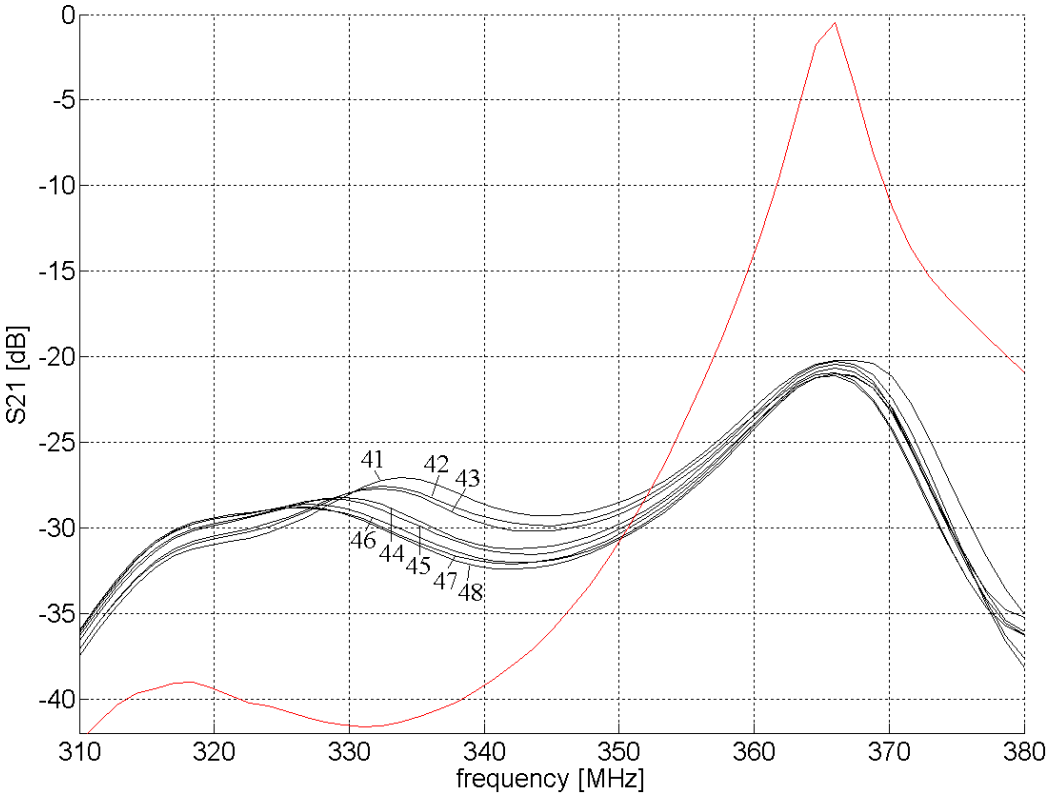

Figure A.6. Resonance curves and the corresponding sample numbers 41-48.

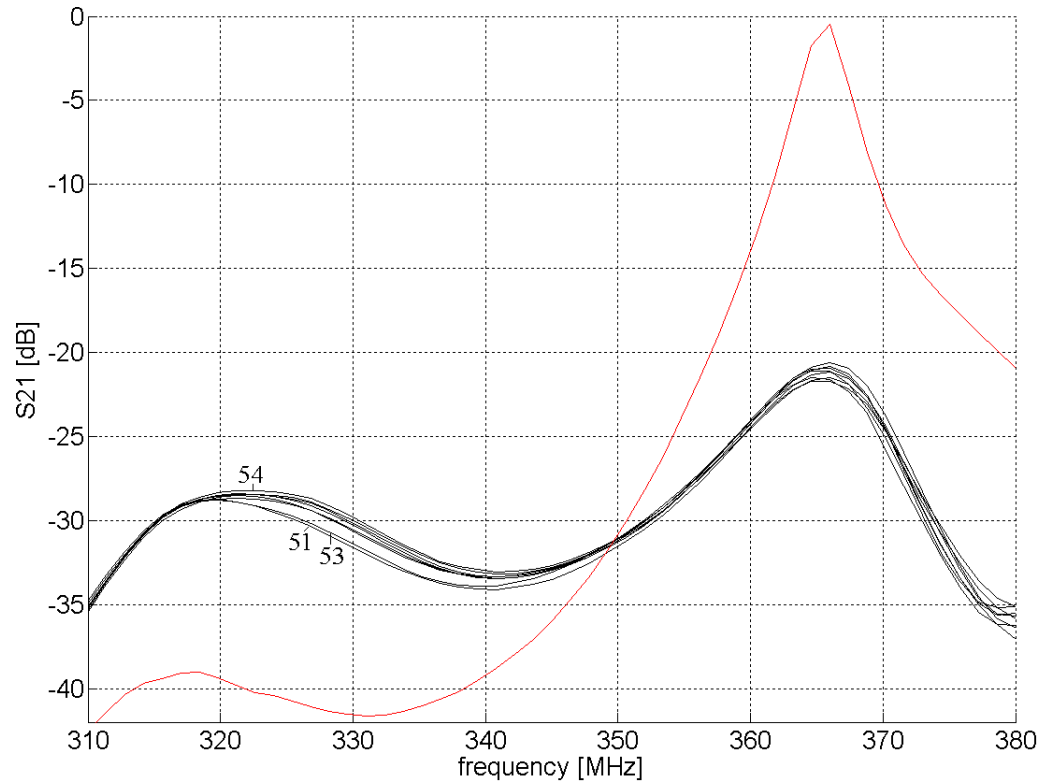

Figure A.7. Resonance curves and the corresponding sample numbers 49-56.

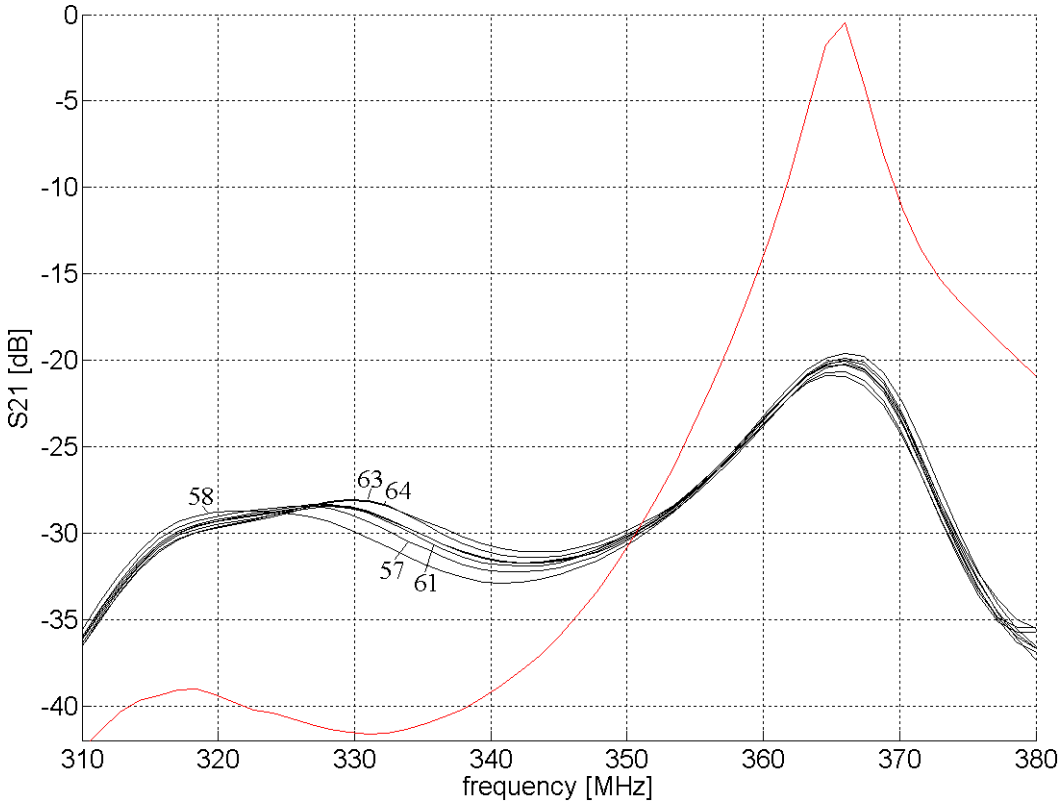

Figure A.8. Resonance curves and the corresponding sample numbers 57-64.

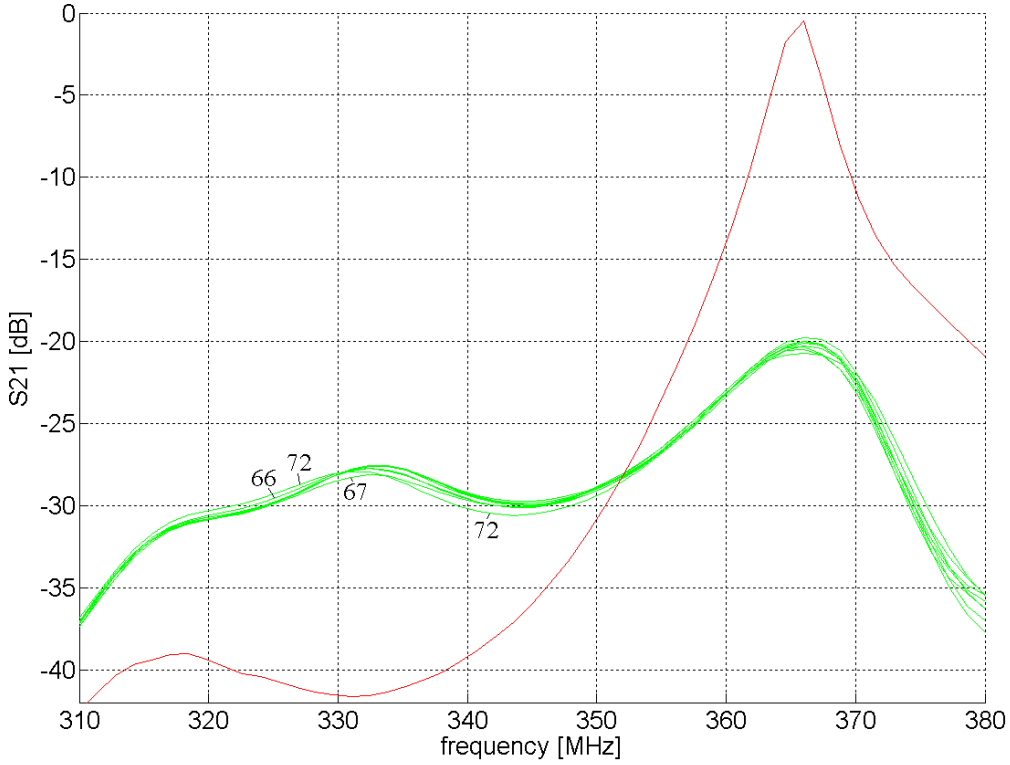

Figure A.9. Resonance curves and the corresponding sample numbers 65-72.

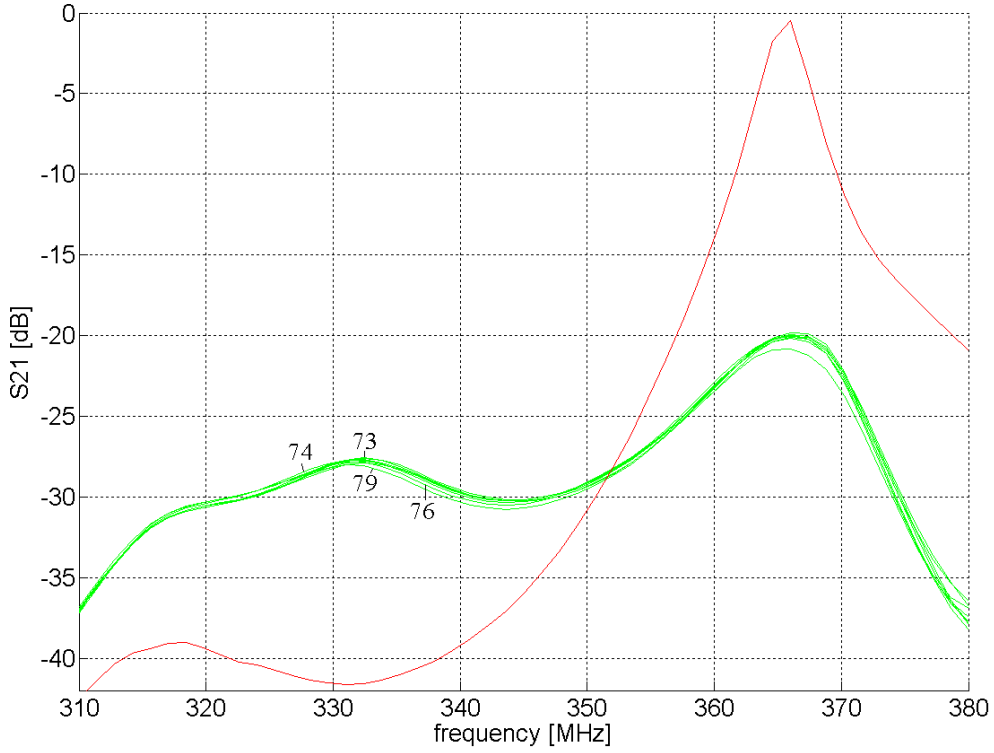

Figure A.10. Resonance curves and the corresponding sample numbers 73-80.

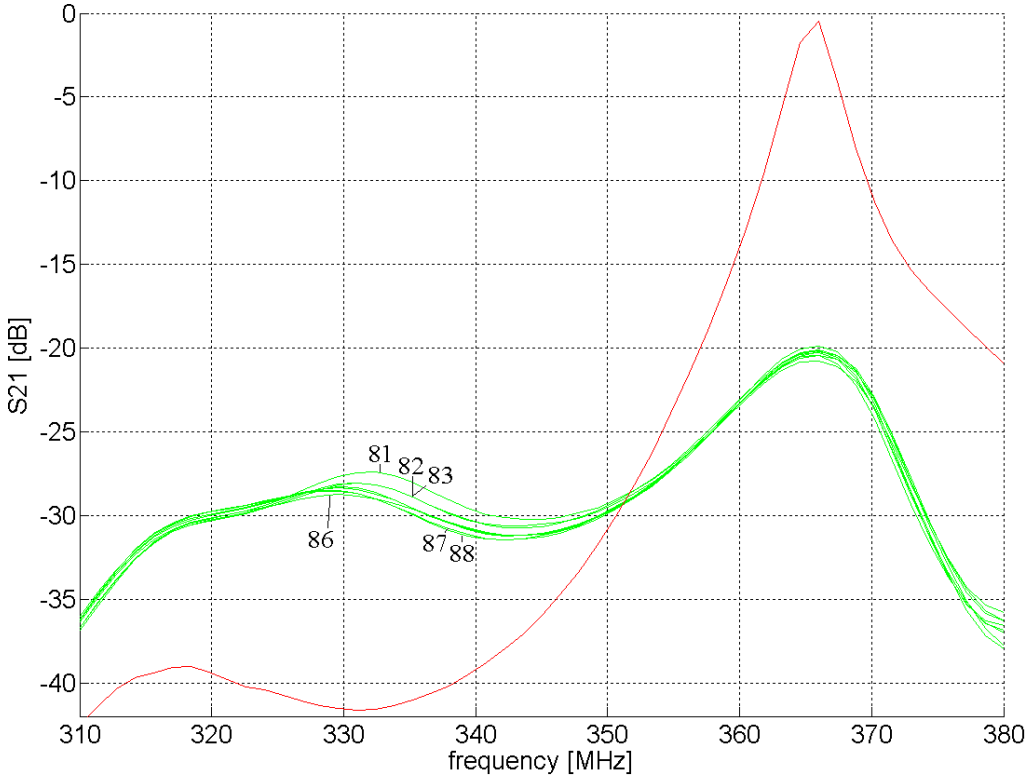

Figure A.11. Resonance curves and the corresponding sample numbers 81-88.

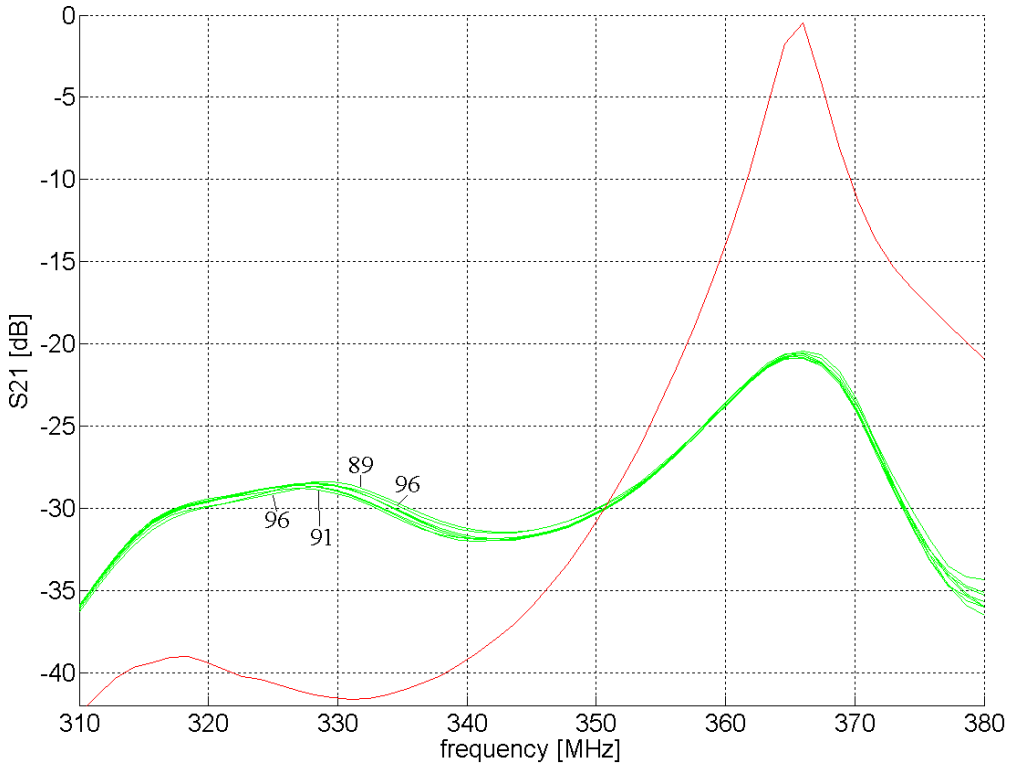

Figure A.12. Resonance curves and the corresponding sample numbers 89-96.

APPENDIX B

DATA OF THE MEASUREMENTS AND THE REFERENCE SAMPLES

Table B.1. Moisture contents (% of weight) dried in the factory.

Sample	Moisture (%)	**Sample**	Moisture (%)	**Sample**	Moisture (%)	**Sample**	Moisture (%)
0	0.560718	**24**	0.561586	**48**	0.552268	**72**	0.567019
1	0.57079	**25**	0.563726	**49**	0.552309	**73**	0.566189
2	0.554511	**26**	0.569367	**50**	0.553023	**74**	0.556601
3	0.575611	**27**	0.572715	**51**	0.552913	**75**	0.571267
4	0.590195	**28**	0.570607	**52**	0.552184	**76**	0.563794
5	0.624752	**29**	0.57417	**53**	0.551959	**77**	0.565413
6	0.571478	**30**	0.575466	**54**	0.558264	**78**	0.558053
7	0.541655	**31**	0.593338	**55**	0.560541	**79**	0.559512
8	0.555064	**32**	0.575588	**56**	0.552379	**80**	0.568643
9	0.577598	**33**	0.577529	**57**	0.557771	**81**	0.560691
10	0.55451	**34**	0.586938	**58**	0.566625	**82**	0.559292
11	0.599228	**35**	0.585095	**59**	0.563346	**83**	0.553054
12	0.569109	**36**	0.594449	**60**	0.561915	**84**	0.565133
13	0.570479	**37**	0.571949	**61**	0.567945	**85**	0.554915
14	0.557018	**38**	0.575158	**62**	0.560017	**86**	0.558006
15	0.563447	**39**	0.561722	**63**	0.568158	**87**	0.553452
16	0.552138	**40**	0.589125	**64**	0.574261	**88**	0.55949
17	0.575082	**41**	0.567932	**65**	0.559496	**89**	0.556405
18	0.527235	**42**	0.545452	**66**	0.565157	**90**	0.56147
19	0.579017	**43**	0.55535	**67**	0.55716	**91**	0.563939
20	0.567082	**44**	0.555392	**68**	0.565964	**92**	0.555319
21	0.550666	**45**	0.551006	**69**	0.553552	**93**	0.559939
22	0.554921	**46**	0.559459	**70**	0.565522	**94**	0.556177
23	0.596587	**47**	0.55811	**71**	0.561652	**95**	0.55961
						96	0.552396

Table B.2. Moisture contents (% of weight) of the samples measured in Aalto University.

Sample	Moisture (%)	Sample	Moisture (%)	Sample	Moisture (%)
0	0.617935	**22**	0.571642	**44**	0.57373
1	0.57379	**23**	0.614895	**45**	0.576949
2	0.538014	**24**	0.573938	**46**	0.570534
3	0.553455	**25**	0.573415	**47**	0.573878
4	0.587087	**26**	0.56353	**48**	0.5758
5	0.63167	**27**	0.572935	**49**	0.575113
6	0.587467	**28**	0.5709	**50**	0.572525
7	0.559667	**29**	0.565235	**51**	0.571745
8	0.559	**30**	0.571418	**52**	0.571491
9	0.562602	**31**	0.590147	**53**	0.566505
10	0.569256	**32**	0.574752	**54**	0.56703
11	0.587525	**33**	0.579182	**55**	0.573803
12	0.56908	**34**	0.598399	**56**	0.569565
13	0.56764	**35**	0.601147	**57**	0.574646
14	0.567091	**36**	0.606893	**58**	0.584469
15	0.576212	**37**	0.572751	**59**	0.582005
16	0.555327	**38**	0.600091	**60**	0.580719
17	0.563179	**39**	0.586844	**61**	0.577277
18	0.578012	**40**	0.590164	**62**	0.575197
19	0.581107	**41**	0.571973	**63**	0.575295
20	0.553117	**42**	0.564292	**64**	0.592076
21	0.571812	**43**	0.564195		

Table B.3. Thicknesses of samples 0 to 96.

Sample	Thickness [mm]	**Sample**	Thickness [mm]	**Sample**	Thickness [mm]	**Sample**	Thickness [mm]
0	10.16667	**24**	13.56667	**48**	13.8	**72**	10.33333
1	20.9	**25**	13.4	**49**	14.03333	**73**	11.44
2	21.36667	**26**	13.36667	**50**	14	**74**	11.14333
3	14.36667	**27**	13.06667	**51**	14.16667	**75**	10.85
4	9.5	**28**	12.9	**52**	14.46667	**76**	11.15
5	7.033333	**29**	12.93333	**53**	13.86667	**77**	10.71
6	8.7	**30**	12.6	**54**	13.66667	**78**	11.09667
7	13.2	**31**	11.83333	**55**	14.13333	**79**	10.90667
8	13.2	**32**	12.06667	**56**	13.73333	**80**	11.39333
9	9.3	**33**	8.733333	**57**	13.18333	**81**	11.37333
10	12.5	**34**	7.883333	**58**	12.93333	**82**	11.84333
11	13.4	**35**	8.433333	**59**	12.36667	**83**	11.94667
12	13.36667	**36**	8.666667	**60**	12.76667	**84**	11.68333
13	13.66667	**37**	8.933333	**61**	12.33333	**85**	12.09667
14	14.16667	**38**	8.533333	**62**	12.56667	**86**	11.86
15	15	**39**	8.366667	**63**	12.78333	**87**	11.98667
16	16.06667	**40**	7.9	**64**	11.53333	**88**	11.90667
17	14.53333	**41**	10.63333	**65**	11.05333	**89**	12.35
18	14.9	**42**	11.66667	**66**	11.63	**90**	12.34333
19	13.36667	**43**	12.6	**67**	10.70667	**91**	11.64333
20	13.53333	**44**	12.9	**68**	10.27	**92**	12.08667
21	14.26667	**45**	12.46667	**69**	10.71	**93**	12.47333
22	13.8	**46**	13.93333	**70**	10.98	**94**	12.57333
23	12.56667	**47**	13.3	**71**	10.08667	**95**	11.81667
						96	12.44333

Table B.4. Data of sample numbers 0 to 64.

Sample	Height of the equivalent water layer h_w [mm]	The relation of h_w and the thickness of the MUT h_w/h_{MUT}	The change in the resonant frequency caused by the MUT Δf_r [MHz]	The relative change in the resonant frequency $\Delta f_r/f_r$	The slope calculated from $(\Delta f_r/f_r)$ / h_w
0	5.383626	0.529537	26.6	0.072678	0.0135
1	10.16429	0.486329	49	0.13388	0.013172
2	4.451106	0.20832	49	0.13388	0.030078
3	11.59713	0.807225	39.2	0.107104	0.009235
4	4.76	0.501053	28	0.076503	0.016072
5	4.664103	0.663143	26.6	0.072678	0.015582
6	4.976852	0.572052	25.2	0.068852	0.013834
7	6.883208	0.521455	37.8	0.103279	0.015004
8	6.81716	0.516451	26.6	0.072678	0.010661
9	4.768056	0.512694	19.6	0.053552	0.011231
10	6.371901	0.509752	37.8	0.103279	0.016209
11	6.685714	0.498934	37.8	0.103279	0.015448
12	6.594286	0.493338	39.2	0.107104	0.016242
13	7.177647	0.525194	37.8	0.103279	0.014389
14	7.75619	0.547496	42	0.114754	0.014795
15	7.97672	0.531781	46.2	0.12623	0.015825
16	7.208556	0.448665	47.6	0.130055	0.018042
17	7.363	0.506628	46.2	0.12623	0.017144
18	8.839827	0.593277	46.2	0.12623	0.01428
19	8.02	0.6	43.4	0.118579	0.014785
20	7.289256	0.538615	43.4	0.118579	0.016268
21	7.056642	0.494624	42	0.114754	0.016262
22	7.304762	0.529331	40.6	0.110929	0.015186
23	7.370909	0.586544	39.2	0.107104	0.014531
24	7.230839	0.532986	30.8	0.084153	0.011638
25	6.75125	0.503825	37.8	0.103279	0.015298
26	6.69899	0.501171	39.2	0.107104	0.015988
27	7.336429	0.561461	37.8	0.103279	0.014078
28	6.718817	0.520839	40.6	0.110929	0.01651
29	7.167965	0.554224	36.4	0.099454	0.013875
30	6.660774	0.528633	36.4	0.099454	0.014931
31	6.824242	0.576697	37.8	0.103279	0.015134
32	6.488696	0.537737	37.8	0.103279	0.015917
33	4.695238	0.537623	25.2	0.068852	0.014664
34	4.891358	0.620468	25.2	0.068852	0.014076
35	5.295789	0.627959	26.6	0.072678	0.013724
36	5.618095	0.648242	26.6	0.072678	0.012936
37	5.006364	0.560414	26.6	0.072678	0.014517
38	5.019048	0.58817	26.6	0.072678	0.01448
39	5.243537	0.626718	26.6	0.072678	0.01386
40	4.834286	0.611935	25.2	0.068852	0.014242
41	5.965385	0.561008	32.2	0.087978	0.014748
42	6.261988	0.536742	33.6	0.091803	0.01466
43	6.72716	0.533902	33.6	0.091803	0.013647

44	6.410476	0.496936	36.4	0.099454	0.015514
45	6.93641	0.556397	37.8	0.103279	0.014889
46	7.474	0.536411	39.2	0.107104	0.01433
47	7.187368	0.540404	39.2	0.107104	0.014902
48	7.223443	0.523438	39.2	0.107104	0.014827
49	7.346405	0.523497	44.8	0.122404	0.016662
50	7.378947	0.527068	43.4	0.118579	0.01607
51	7.5375	0.532059	46.2	0.12623	0.016747
52	7.874	0.544286	44.8	0.122404	0.015545
53	7.453711	0.537527	46.2	0.12623	0.016935
54	7.343653	0.53734	43.4	0.118579	0.016147
55	6.939	0.490967	44.8	0.122404	0.01764
56	7.86	0.57233	44.8	0.122404	0.015573
57	6.700277	0.508238	39.2	0.107104	0.015985
58	7.473684	0.577862	44.8	0.122404	0.016378
59	7.088889	0.573226	37.8	0.103279	0.014569
60	6.64125	0.520202	37.8	0.103279	0.015551
61	6.755238	0.547722	39.2	0.107104	0.015855
62	6.835714	0.543956	37.8	0.103279	0.015109
63	6.458095	0.505196	36.4	0.099454	0.0154
64	7.263	0.62974	36.4	0.099454	0.013693

Table B.5. Data of the samples after thickness calibration. Only the samples that are taken into account in the thickness calibration of the resonator are listed.

Sample	The relative change in the resonant frequency $\Delta f_r/f_r$	Height of the equivalent water layer h_w [mm]	The slope calculated from $(\Delta f_r/f_r)$ / h_w
0	0.072678	5.383626	0.0135
3	0.107104	11.59713	0.009235
7	0.103279	6.883208	0.015004
8	0.072678	6.81716	0.010661
10	0.103279	6.371901	0.016209
11	0.103279	6.685714	0.015448
12	0.107104	6.594286	0.016242
13	0.103279	7.177647	0.014389
14	0.114754	7.75619	0.014795
15	0.12623	7.97672	0.015825
16	0.130055	7.208556	0.018042
17	0.12623	7.363	0.017144
18	0.12623	8.839827	0.01428
19	0.118579	8.02	0.014785
20	0.118579	7.289256	0.016268
21	0.114754	7.056642	0.016262
22	0.110929	7.304762	0.015186
23	0.107104	7.370909	0.014531
24	0.084153	7.230839	0.011638
25	0.103279	6.75125	0.015298
26	0.107104	6.69899	0.015988
27	0.103279	7.336429	0.014078
28	0.110929	6.718817	0.01651
29	0.099454	7.167965	0.013875
30	0.099454	6.660774	0.014931
31	0.103279	6.824242	0.015134
32	0.103279	6.488696	0.015917
41	0.087978	5.965385	0.014748
42	0.091803	6.261988	0.01466
43	0.091803	6.72716	0.013647
44	0.099454	6.410476	0.015514
45	0.103279	6.93641	0.014889
46	0.107104	7.474	0.01433
47	0.107104	7.187368	0.014902
48	0.107104	7.223443	0.014827
49	0.122404	7.346405	0.016662
50	0.118579	7.378947	0.01607
51	0.12623	7.5375	0.016747
52	0.122404	7.874	0.015545

53	0.12623	7.453711	0.016935
54	0.118579	7.343653	0.016147
55	0.122404	6.939	0.01764
56	0.122404	7.86	0.015573
57	0.107104	6.700277	0.015985
58	0.122404	7.473684	0.016378
59	0.103279	7.088889	0.014569
60	0.103279	6.64125	0.015551
61	0.107104	6.755238	0.015855
62	0.103279	6.835714	0.015109
63	0.099454	6.458095	0.0154
64	0.099454	7.263	0.013693